UNIVERSIDADE ESTADUAL DE CAMPINAS
Faculdade de Engenharia Mecânica

Julio Alves Mesquita da Silva

Study and application of min-type control strategies in DC-DC power converters

Estudo e aplicação de estratégias de controle do tipo mínimo em conversores de potência CC-CC

Campinas
2021

Julio Alves Mesquita da Silva

Study and application of min-type control strategies in DC-DC power converters

Estudo e aplicação de estratégias de controle do tipo mínimo em conversores de potência CC-CC

Dissertation presented to the School of Mechanical Engineering of the University of Campinas in partial fulfillment of the requirements for the degree of Master in Mechanical Engineering, in the area of Mechatronics.

Dissertação apresentada à Faculdade de Engenharia Mecânica da Universidade Estadual de Campinas como parte dos requisitos para a obtenção do título de Mestre em Engenharia Mecânica, na área de Mecatrônica.

Orientador: Prof. Dr. Tárcio André dos Santos Barros
Coorientadora: Profa. Dra. Grace Silva Deaecto

Este exemplar corresponde à versão da Dissertação entregue à banca antes da defesa.

Campinas
2021

Ficha catalográfica
Universidade Estadual de Campinas
Biblioteca da Área de Engenharia e Arquitetura
Rose Meire da Silva - CRB 8/5974

Si38s Silva, Julio Alves Mesquita da, 1996-
Study and application of min-type control strategies in DC-DC power converters / Julio Alves Mesquita da Silva. – Campinas, SP : [s.n.], 2021.

Orientador: Tárcio André dos Santos Barros.
Coorientador: Grace Silva Deaecto.
Dissertação (mestrado) – Universidade Estadual de Campinas, Faculdade de Engenharia Mecânica.

1. Conversores de potência. 2. Funções de Lyapunov. 3. Controle robusto. 4. Sistemas de Comutação. 5. Teoria de comutação. I. Barros, Tárcio André dos Santos, 1987-. II. Deaecto, Grace Silva, 1983-. III. Universidade Estadual de Campinas. Faculdade de Engenharia Mecânica. IV. Título.

Informações para Biblioteca Digital

Título em outro idioma: Estudo e aplicação de estratégias de controle do tipo mínimo em conversores de potência CC-CC
Palavras-chave em inglês:
Power converters
Lyapunov functions
Robust control
Switching systems
Switching theory
Área de concentração: Mecatrônica
Titulação: Mestre em Engenharia Mecânica
Banca examinadora:
Tárcio André dos Santos Barros [Orientador]
Vilma Alves de Oliveira
Alfeu Joãozinho Sguarezi Filho
Data de defesa: 08-03-2021
Programa de Pós-Graduação: Engenharia Mecânica

Identificação e informações acadêmicas do(a) aluno(a)
- ORCID do autor: https://orcid.org/0000-0001-7246-8663
- Currículo Lattes do autor: http://lattes.cnpq.br/2061086831058835

FOLHA DE APROVAÇÃO

Abaixo se apresentam os membros da comissão julgadora da sessão pública de defesa de dissertação para o Título de Mestre em Engenharia Mecânica na área de concentração Mecatrônica, a que se submeteu o aluno Julio Alves Mesquita da Silva, em 08 de março de 2021 na Faculdade de Engenharia Mecânica – FEM/UNICAMP, em Campinas/SP.

Prof. Dr. Tárcio André dos Santos Barros
Presidente da Comissão Julgadora

Profa. Dra. Vilma Alves de Oliveira
Escola de Engenharia de São Carlos/USP

Prof. Dr. Alfeu Joãozinho Sguarezi Filho
Centro de Engenharia, Modelagem e Ciências Sociais Aplicadas/UFABC

Ata da defesa, assinada pelos membros da Comissão Examinadora, consta no SIGA/Sistema de Fluxo de Dissertação/Tese e na Secretaria de Pós Graduação da FEM.

Acknowledgements

I would like to express my deepest appreciation to Tárcio and Grace for their valuable teachings and their overall support. This work wouldn't be possible without them.

I'm extremely grateful to FAEPEX for the financial aid. They allowed me to fully dedicate to this work.

I would also like to thank my family and friends for the support throughout this phase.

Resumo

Essa dissertação consiste em generalizar algumas regras de comutação do tipo mínimo, disponíveis na literatura, para levar em conta robustez com relação à mudança de ponto de equilíbrio e variação na carga de saída, de forma a deixá-las mais adaptadas para aplicações práticas em engenharia, como é caso do controle de conversores de potência CC-CC. Estas regras são as únicas variáveis de controle atuando no sistema e são projetadas de forma a assegurar estabilidade e desempenho adequado para o mesmo. Muitas técnicas de controle baseadas em regras desta classe foram desenvolvidas nos últimos anos, porém, até o momento, não foi realizada uma análise detalhada a respeito da sua eficiência e desempenho em aplicações reais. Esta análise é importante pois nos permite avaliar se estas novas técnicas são alternativas viáveis em relação às opções já existentes na literatura. Ao longo do estudo, vamos comparar três regras de chaveamento do tipo mínimo distintas. Mais especificamente, duas são desenvolvidas no domínio do tempo contínuo e exigem frequências de chaveamento arbitrariamente altas. A outra é mais realista, pois permite considerar frequências de chaveamento limitadas, sendo obtidas a partir de condições de projeto para sistemas a tempo discreto. Todas elas são derivadas de trabalhos anteriores, porém, com novas adaptações. Essas adaptações objetivam tornar o controlador robusto, tanto a variações de carga quanto a variações de tensão de saída. Para melhor avaliação comparamos as estratégias de controle do tipo mínimo com o controlador PI clássico, comumente utilizado na literatura.

Ao longo desse estudo, nós analisamos o comportamento nos regimes transitório e permanente destas regras de chaveamento para três conversores distintos. Para o buck, o boost, e o buck-boost. A modelagem de cada um dos conversores é abordada, assim como a metodologia de projeto para cada técnica de controle estudada. Por meio de simulações e testes experimentais, nós apresentamos o comportamento dos conversores operando sob a atuação de cada uma das metodologias de controle, ressaltando as vantagens e desvantagens de cada uma delas. Outro resultado importante é proveniente da análise da frequência de chaveamento que, sob a influência de regras do tipo mínimo, pode variar consideravelmente dependendo da tensão de saída desejada. Esses perfis de frequência indicam um grande potencial para redução de perdas por chaveamento no conversor aumentando, assim, sua eficiência.

Palavras Chave — Conversores de potência, Funções de Lyapunov, Controle robusto, Sistemas de comutação, Teoria de comutação

Abstract

This dissertation consists of the generalization of some available min-type switching rules to cope with changes in the equilibrium point and output load variation, making them more amenable for practical implementations in engineering, as is the case of the DC-DC power converters control. These rules are the unique control variable acting in the system and are designed in order to assure stability and suitable performance for it. Many of the control techniques based on rules of this class have been developed in recent years. However, there is a lack in the literature concerning a detailed analysis of their efficiency and performance in real applications. This analysis is important to evaluate if these new techniques are viable alternatives with respect to the options already existent in the literature. Throughout the study, we will compare three distinct min-type switching rules. More specifically, two are developed in continuous time and require arbitrarily high switching frequencies. The other is more realistic since it allows us to consider limited switching frequency and is obtained from design conditions developed for discrete-time systems. All of them are derived from previous works, but with new adaptations. These adaptations aim to make the controller robust concerning load and output voltage variations, making them a viable option compared to usual techniques. For a better evaluation, we have compared the min-type switching strategies with the classical PI controller, commonly adopted in the literature.

Throughout this study, we have verified the control strategies behavior in three different converters: buck, boost, and buck-boost. The modeling of each converter is covered as well as the design methodology for each control technique. Using simulations and experimental tests, we have presented the converters' behavior in the transient and steady-state, highlighting the advantages and disadvantages of each technique. Another significant result comes from analyzing the switching frequency, which under min-type switching strategies can vary considerably according to the desired output voltage. These frequency profiles indicate a great potential for reducing losses in the converter due to the switching, thus increasing its efficiency.

Keywords — Power Converters, Lyapunov functions, Robust control, Switching systems, Switching theory

List of Figures

List of Symbols

I	Identity matrix.
N	Number of subsystems.
$\mathbb{K}$	Set $\{1, \dots, N\}$ of the first N natural numbers.
$\mathbb{R}$	Set of real numbers.
$\mathbb{R}^{m \times n}$	Set of real numbers with dimension $m \times n$.
Λ	Unit simplex $\Lambda = \{\lambda \in \mathbb{R}^N \mid \lambda_j \geq 0 \text{ and } \sum_{j=1}^{N} \lambda_j = 1\}$.
X_λ	The convex combination $X_\lambda = \sum_{i \in \mathbb{K}} \lambda_i X_i$.
X'	Transpose of the X matrix.
$\dot{x}$	Time derivative of the state x.
$\mathrm{Tr}(\bullet)$	Trace function.
$X > 0$	Positive definite real and symmetric matrix.
$X < 0$	Negative definite real and symmetric matrix.
δ	Duty-cycle of a PWM signal.

Contents

Chapter 1

Introduction

DC-DC converters are widely studied and used in the field of power electronics. Their applications extend from the activation of motors [29] to the voltage regulation of photovoltaic modules [32]. In all of these cases, the voltage generated by the converter should remain stable at the desired value. This value must be maintained steady both in the event of a supply voltage variation and cases where the load varies. One way to achieve this objective is through a suitable control design.

Control is an essential part of the field of power electronics. The goal is to design a controller to assure stability, rapid transient response, robustness, and an extensive, reliable operation range. To achieve these requirements, the scientific community is continuously developing new and more efficient control techniques, which must provide not only good performance but also be easy to implement.

In general, DC-DC power converters can be modeled as switched affine systems, characterized by a set of affine subsystems and a rule orchestrating the switching among them. The control of their electronic switches follows a specific rule designed to regulate the output voltage. Nowadays, most of the switching logic relies on a classical controller, which is determined taking into account a Linear Time-Invariant (LTI) averaged model, which describes the behavior of the switched system for a specific operation point. Through this logic, the duty-cycle of a Pulse Width Modulation (PWM) signal is dynamically adjusted, regulating the voltage. Although this is a well-known and widely used technique, there is still room for improvements, mainly when the control design is based directly on the original switched system, without any approximation for averaged models.

The literature provides several works focused on improving the PWM-based controllers, such as [2, 23, 24]. In general, these studies propose slight changes compared to classical control methodologies. However, some researchers approached the problem differently and proposed control strategies based on the theory of hybrid systems, such as sliding mode control [25, 31], or based on a switching table procedure [8]. Another relatively novel approach is the control based on min-type switching rules, in which we will focus on this study. There are already a significant number of articles on this subject mainly motivated by issues and concerns raised in practical applications of the power electronics domain (see [5, 13, 15]). Reference [10] was one of the first in proposing sufficient conditions for the design of min-type switching functions to assure global asymptotic stability of switched affine systems based on the Lyapunov theory. The study applied the control methodology to regulate the output voltage of standard DC-DC power converters through simulation. However, an issue observed in this technique is an arbitrarily high switching frequency requirement to assure asymptotic stability. The experimental validation of the control technique proposed in [10] has been presented in [15], which applied the min-type switching functions on a boost converter. Other than merely demonstrating experimental results, [15] also explored the Lyapunov matrix design and different switching rules. The article also proposed two techniques to operate the converter with partial information of the equilibrium point. The first is the use of a low pass filter to estimate the equilibrium current. The second uses an integrator to determine the equilibrium current based on the output voltage error.

The generalization of these results to consider a limited switching frequency to avoid chattering was proposed in [11], but only for the more straightforward case where the subsystems are linear. Chattering is an undesirable phenomenon that can damage pieces of equipment and is a problem to be avoided during the control design. Reference [11] has proposed a robust control design for a discrete-time switched linear system, which is equivalent to the continuous-time one and comes from the solution of Riccati–Metzler inequalities. With discrete-time models, the switching may occur only at the sampling times, which occurs at a fixed rate.

In a more general framework, references [9, 13] have proposed switching rules with limited frequency for switched affine systems based on discrete-time models. In this case, it is no longer possible to guarantee asymptotic stability. Therefore, the proposed methodologies are focused on assuring practical stability, where the state trajectories are governed to an invariant set of attraction as small as possible, containing the desired equilibrium point. Generally, the objective function is to minimize the volume of this set to make the steady-state behavior of the state trajectories as near as possible the desired equilibrium. Unfortunately, nothing can be concluded regarding these trajectories inside the set of attraction, and it is not possible to impose $\mathcal{H}_2$ and $\mathcal{H}_\infty$ performance indexes. To circumvent these difficulties, references [12, 27] tried to shift the paradigm once more. Instead of making the system attain one specific equilibrium point, these strategies aim to make the converter follow a predefined limit cycle. In this case, the limit cycle is designed to satisfy steady-state criteria of interest. Moreover, the switching rule can assure asymptotic stability of the designed limit cycle, which allowed [12] to take into account $\mathcal{H}_2$ and $\mathcal{H}_\infty$ performance indexes.

Considering the state of the art for switched affine systems, this dissertation relies on previously designed switching rules and proposes important generalizations. The objective is to make these switching rules robust to changes in the equilibrium point and load variations without requiring redesign, making them an efficient alternative for real applications. The idea is to provide novel stability conditions as close as possible to the original ones without introducing great conservativeness. The transient and steady-state responses were analyzed, and the performance of these switching rules was compared with the ones derived from classical controllers. We also explored the control techniques' capabilities regarding power loss reduction. In the next section, an outline of the chapters is presented, explaining the approached contents in further detail.

1.1 Publication

This dissertation is partly based on the paper:

J. A. M. Silva, G. S. Deaecto, and T. A. S. Barros. "Analysis and Design Aspects of Min-Type Switching Control Strategies for Synchronous Buck-Boost Converter". In: *Journal of Emerging and Selected Topics in Power Electronics* (submitted)

1.2 Outline of the Chapters

- **Chapter 2:** Presents some fundamental concepts important for this study. Its content includes the stability of linear time-invariant systems, an introduction about switched affine systems, and a brief about DC-DC power converters. It includes the topologies of each converter, as well as their mathematical models. Some relevant equations are also developed to help with the control design and implementation. The objective is to supply the readers with the needed mathematical tools to understand and potentially replicate the dissertation results.

- **Chapter 3:** During this chapter, we present the control strategies considered in this study and their generalization to take into account changes in the equilibrium points and load variations. We have also presented the PWM-based technique that serves as a comparison for the min-type controllers, which are our main focus in this dissertation. Two steady-state correction methods have been proposed to compensate for any unmodeled behavior. With their help, the converter attains the reference voltage without any steady-state error.

- **Chapter 4:** In this chapter, the experimental converter build is presented, as well as an overview of its simulations. All the controllers were designed and provided throughout the chapter. More specifically, we presented the designed parameters for each min-type control strategy. Graphs showing several important aspects of practical applications have been presented, including comparisons with the classical method.

- **Chapter 5:** Discusses the variable frequency aspect of the min-type controllers. The focus is on analyzing the frequency patterns and their variation according to changes in the output load and voltage. The objective is to discuss how applications may use these control strategies to reduce the power losses caused by the switching.

- **Chapter 6:** Recaps the previous chapters and the main points presented throughout the study. The most important contributions are revisited. Opportunities for future works are also highlighted.

Chapter 2

Fundamentals

This chapter presents some fundamental concepts that are important for the forthcoming chapters. More specifically, we provide the state space representation of an affine time-invariant system in the continuous and discrete-time domains and the discretization methodology adopted in this dissertation. Afterward, a brief introduction about switched affine systems is provided, highlighting their main characteristics. In the end, we present the DC-DC power converters of interest, discussing the topologies of each converter and their mathematical models. Some relevant equations are also developed to help with the control design and implementation.

2.1 Affine Time Invariant Systems

The state-space representation of an affine time-invariant system of order n is given by a set of n differential equations of first order, which is expressed in the matrix form as

$$\begin{cases} \dot{x}(t) = Ax(t) + Bu, \;\; x(0) = x_0 \\ z(t) = Cx(t) + Du \end{cases} \tag{2.1}$$

where $x(t) \in \mathbb{R}^n$ is the state, $u \in \mathbb{R}^m$ is a constant input signal, and $z \in \mathbb{R}^p$ is the controlled output. The matrices $A \in \mathbb{R}^{n \times n}$, $B \in \mathbb{R}^{n \times m}$, $C \in \mathbb{R}^{p \times n}$ and $D \in \mathbb{R}^{p \times m}$ are constant matrices which define the system behavior. If the matrix A is Hurwitz stable, the equilibrium point is given by

$$x_e = -A^{-1}Bu \tag{2.2}$$

obtained by making $\dot{x} = 0$. Although, the model in continuous-time domain is important because expresses closely the system behavior in real time, its representation in the discrete-time domain seems more appropriate for control design purposes. This occurs because nowadays most of the controllers is embedded and act on the system digitally respecting a certain sampling period $T > 0$.

Considering a time instant $t \in [t_k, t_{k+1})$ with $t_{k+1} - t_k = T$, from the dynamic equation in (2.1), we have

$$\begin{aligned} x(t) &= e^{A(t-t_k)} x(t_k) + \int_{t_k}^{t} e^{A(t-\tau)} \, d\tau \, Bu \\ &= e^{A(t-t_k)} x(t_k) + \int_{0}^{t-t_k} e^{A\psi} \, d\psi \, Bu \end{aligned}$$

valid for $t \in [t_k, t_{k+1})$, where it has been adopted the change of variable $\psi = t - \tau$. Hence, at the sampling instants we obtain

$$x(t_{k+1}) = e^{AT} x(t_k) + \int_0^T e^{A\psi} \, d\psi \, Bu$$

which allow us to determine the dynamic equation in the discrete-time domain given by

$$\begin{cases} x[k+1] = Fx[k] + Gu[k], \;\; x[0] = x_0 \\ \quad z[k] = Hx[k] + Ju[k] \end{cases} \tag{2.3}$$

with

$$F = e^{AT}, \;\; G = \int_0^T e^{A\tau} d\tau \, B \tag{2.4}$$

and discrete-time output matrices obtained as

$$\int_0^T e^{\mathcal{A}'t} \mathcal{C}' \mathcal{C} e^{\mathcal{A}'t} dt = \begin{bmatrix} H' \\ J' \end{bmatrix} \begin{bmatrix} H' \\ J' \end{bmatrix}', \;\; \mathcal{A} = \begin{bmatrix} A & B \\ 0 & 0 \end{bmatrix}, \;\; \mathcal{C} = \begin{bmatrix} C & D \end{bmatrix} \tag{2.5}$$

see [7] for further details about this discretization. Notice that, the discretization is an exact representation of the continous-time system at the sampling instants and the equilibrium point is

$$y_e = (I - F)^{-1} Gu \tag{2.6}$$

which tends to the continuous time equilibrium point for T arbitrarily small. Indeed, in this case, we have

$$e^{AT} \approx I + AT, \int_0^T e^{A\tau} d\tau \approx T \tag{2.7}$$

which leads to

$$y_e = (I - F)^{-1} G u \approx -A^{-1} B u = x_e \tag{2.8}$$

2.2 Switched Affine Systems

Hybrid systems have an intrinsic characteristic of needing continuous and discrete-time dynamics to describe their behavior. Therefore, the system can suffer from changes not describable through a set of continuous-time functions. Due to this characteristic, the classical control design methods are not directly applicable. They require many considerations, making the control of these systems somewhat challenging.

Switched affine systems are a specific type of hybrid systems. In this cases, the discrete-time event that changes the system dynamics is the switching function, which is responsible for selecting one of the N possible subsystems, which are states of operation of the system. Each subsystem can then be described through a set of continuous-time equations. The whole system behavior can be described through the state-space equations

$$\dot{x}(t) = A_\sigma x(t) + B_\sigma u(t), \; x(0) = x_0 \tag{2.9}$$

where $\sigma(t) : t \geq 0 \longrightarrow \mathbb{K} = \{1, \ldots, N\}$ is the switching function responsible for selecting one of the possible subsystems. This model can be further developed to also describe the discrete-time behavior of the system. This property can be mathematically represented as

$$\mathcal{H} : \begin{cases} \begin{bmatrix} \dot{x} \\ \dot{\sigma} \end{bmatrix} = f(x, u, \sigma), & (x, u, \sigma) \in \mathcal{C} \\ \begin{bmatrix} x^+ \\ \sigma^+ \end{bmatrix} \in G(x, u, \sigma), & (x, u, \sigma) \in \mathcal{D} \end{cases} \tag{2.10}$$

where $\mathcal{D}$ is the jump set. If $(x, u, \sigma) \notin \mathcal{D}$ then $(x, u, \sigma) \in C$, representing that the system is to stay at the active subsystem. The flow map f and the jump map G can then be defined by

$$\begin{aligned} f(x, u, \sigma) &:= \begin{bmatrix} A_\sigma x + B_\sigma u \\ 0 \end{bmatrix} \\ G(x, u, \sigma) &:= \begin{bmatrix} x \\ \sigma(x, u) \end{bmatrix} \end{aligned} \tag{2.11}$$

Although the equation (2.9) accurately describes the system, making analyzes with this model is not simple, since its behavior depends on the switching rule $\sigma(t)$. A possible approach is to obtain an averaged system as

$$\dot{x}(t) = A_\lambda x(t) + B_\lambda u(t), \;\; x(0) = x_0 \tag{2.12}$$

that expresses approximately the system behavior associated to an equilibrium point of interest, see [10] and [17]. In the system (2.12) the matrices (A_λ, B_λ) are given by

$$A_\lambda = \sum_{i=1}^{N} \lambda_i A_i, B_\lambda = \sum_{i=1}^{N} \lambda_i B_i \tag{2.13}$$

the vector λ is associated to the equilibrium point of interest and belongs to the unit simplex defined as

$$\Lambda = \{\lambda \in \mathbb{R}^N \; : \; \sum_{i}^{N} \lambda_i = 1, \; \lambda_i > 0\} \tag{2.14}$$

It should be noted that, for switched affine systems, for any given input u, there exist multiple possible equilibrium points composing the set X_e defined as

$$X_e = \{x_e \in \mathbb{R}^n \; : \; x_e = A_\lambda^{-1} B_\lambda u, \; \lambda \in \Lambda\} \tag{2.15}$$

which defines a region of great interest in the space state.

In the context of this dissertation, the switching rule is the unique control variable of the system and, therefore, the control problem consists in determining a switching rule $\sigma(x(t)) : \mathbb{R}^n \longrightarrow \mathbb{K}$ capable of taking the state trajectories from any initial condition x_0 to the desired equilibrium point $x_e \in X_e$.

For the sake of practical applications, it is important to consider a constraint on the switching function in order to impose an upper bound on the switching frequency. In this case, the switching function is modeled as

$$\sigma(t) = \sigma(t_k) = \sigma(Tk) = \sigma[k], \ \forall t \in [t_k, t_{k+1}) \tag{2.16}$$

where $T = t_{k+1} - t_k$ is the sampling period with t_k and t_{k+1} being two successive sampling instants. With the switching function (2.16), it is possible to define the following discrete-time switched affine system

$$x[k+1] = F_\sigma x[k] + G_\sigma u, \ x[0] = x_0 \tag{2.17}$$

whose matrices are determined by solving

$$F_i = e^{A_i T}, \ \ G_i = \int_0^T e^{A_i \tau} d\tau \ B_i \tag{2.18}$$

where A_i and B_i are obtained from the continuous-time model. As proven in [11], the discrete-time system (2.3) is equivalent to the continuous-time one (2.9), whenever $\sigma(t)$ satisfies the constraint (2.16). In this case, the set of attainable equilibrium points is given by

$$Y_e = \{y_e \in \mathbb{R}^2 \ : \ y_e = (I - F_\lambda)^{-1} G_\lambda u, \ \lambda \in \Lambda\} \tag{2.19}$$

It is simple to verify that when $T \longrightarrow 0$ the set Y_e becomes X_e as expected.

2.3 DC-DC Power Converters

Widely used in electrical engineering, power converters are electronic devices whose objective is to change the form, voltage, or frequency of the electric energy. We can classify them into four main groups: DC-DC Converters, DC-AC Converters (Inverters), AC-DC Converters (Rectifiers), and AC-AC converters (Cycloconverters). Throughout this study, we will focus on DC-DC power converters, specifically the switched DC-DC converters. These devices alter a DC source voltage level through an arrangement of switches operating at a sufficiently high frequency.

There is a wide range of converters available and used commercially; however, it is necessary to select a few to serve as objects of study for practicality. As our focus is on the control techniques, we will stick to some already well-known and commonly applied converters, the Buck, the Boost, and the Buck-Boost. All of them are switched DC-DC power converters. As the name suggests, we can model them using the switched affine systems format, enabling the use of the min-type switching strategies presented in Chapter 3.

The topology of each of the converters will be studied and their behavior modeled. Let us define the state variable

$$x(t) = \begin{bmatrix} i_L(t) \\ v_o(t) \end{bmatrix}$$

where i_L and v_o denote the inductor current and output voltage, respectively. Furthermore, for the equilibrium point $x_e = [I_e \ \ V_e]'$, I_e denotes the equilibrium current and V_e the equilibrium voltage, also known as reference voltage.

In this chapter, we will consider converters with the parameters from Table 2.1.

Table 2.1: Parameters for the converters

Parameter	Symbol	Value
Input Voltage (V)	V_s	65
Coil Inductance (mH)	L	1.981
Coil Resistance (Ω)	R	0.49
Output Capacitance (μF)	C_o	2250
Load Resistance (Ω)	R_o	96.8

2.3.1 Buck

The Buck converter, also known as step-down, decreases the voltage supplied by a DC source. This effect is possible through a combination of two states of operation, also referred to as subsystems. In the first stage, the source connects in series to the inductor and the load. After some time, the power source disconnects, leaving the inductor responsible for the output power. The alternation between these states regulates the power transmission.

Figure 2.1 presents the circuit diagram for a synchronous buck converter. We chose a synchronous topology, with two switches instead of one switch and a diode, to better control all state changes. In an asynchronous converter, the system dynamics would change when the inductor current reached zero, making the control design more difficult.

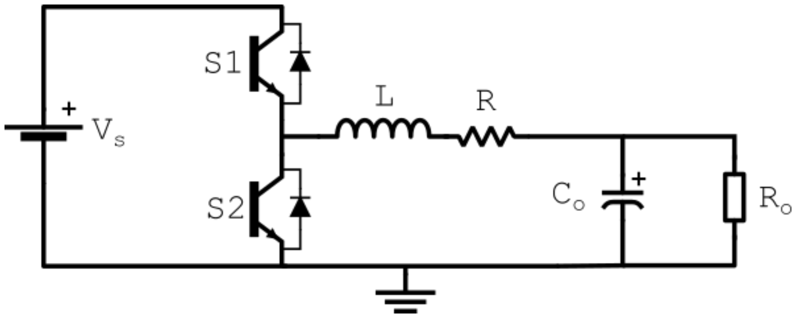

Figure 2.1: Synchronous Buck circuit diagram.

Due to its two switches, their state combinations result in four possible subsystems. However, it is easy to note that the switches (S_1, S_2) cannot stay both active at the same time to avoid short circuits. The state where both are open is also of no interest, as in this case, no power transfer occurs. Therefore, two subsystems remain. The first when S_1 is active, and the second when S_2 is active. Considering these two possibilities, we modeled the system, resulting in the following state-space matrices

$$A_1 = A_2 = \begin{bmatrix} -R/L & -1/L \\ 1/C_o & -1/R_oC_o \end{bmatrix}, \quad B_1 = \begin{bmatrix} 1/L \\ 0 \end{bmatrix}, \quad B_2 = \begin{bmatrix} 0 \\ 0 \end{bmatrix}.$$

The convex combination of these subsystems makes it possible to determine the set of equilibrium points X_e. As was already mentioned in Chapter 3, min-type control strategies require the knowledge of the full equilibrium point to operate. This requirement is not convenient, as the classical method requires only one of these variables as input. Therefore, it would be suitable for the min-type strategies to control the system with the knowledge of only the output voltage. To make this possible, for a specific equilibrium point and its associated

$\lambda \in \Lambda$, the convex combination $A_\lambda x_e + B_\lambda u = 0$ can be manipulated though

$$\begin{aligned}
\begin{bmatrix} I_e \\ V_e \end{bmatrix} &= - \begin{bmatrix} -R/L & -1/L \\ 1/C_o & -1/R_oC_o \end{bmatrix}^{-1} \begin{bmatrix} \lambda_1/L \\ 0 \end{bmatrix} V_s \\
\begin{bmatrix} I_e \\ V_e \end{bmatrix} &= - \begin{bmatrix} \frac{-R\lambda_1}{L} \\ \frac{\lambda_1}{C_oL} \end{bmatrix} \frac{V_s}{\Delta} \\
\begin{bmatrix} \lambda_1 \\ \lambda_1 \end{bmatrix} &= \begin{bmatrix} I_e\frac{L}{R} \\ V_eC_oL \end{bmatrix} \frac{\Delta}{V_s}
\end{aligned} \tag{2.20}$$

where $\Delta = \det(A_\lambda)$. Then the equilibrium variables can be correlated through

$$I_e = \frac{V_e}{R_o} \tag{2.21}$$

In a similar manner, we can also obtain an equation capable of providing the values of λ for a given equilibrium point. By solving the equation (2.20), we obtain

$$\lambda := \begin{cases} \lambda_1 = \frac{V_e + RI_e}{V_s} \\ \lambda_2 = 1 - \lambda_1 \end{cases} \tag{2.22}$$

These results are presented in the graphs of Figure 2.2.

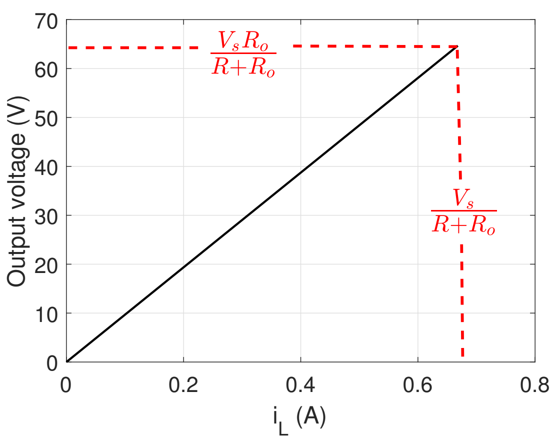

(a) Equilibrium region X_e for the buck converter.

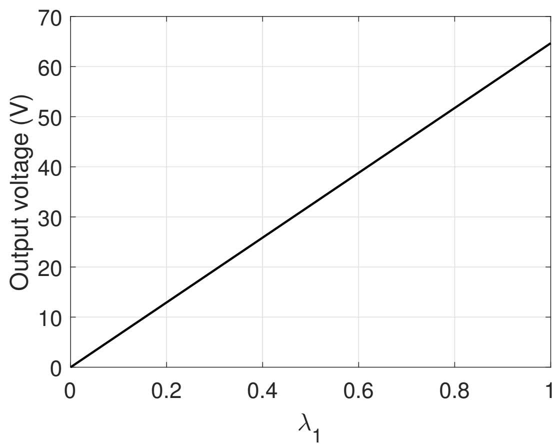

(b) Relation between λ_1 and the equilibrium voltage V_e for the buck converter.

Figure 2.2: Equilibrium region and its relation to λ for the buck converter.

Most of the equations and matrices determined until this point are only needed for the switched affine model. However, as will be further explored in Chapter 3, the design of a classical controller requires a LTI model of the type $G(s) = \hat{V}_o(s)/\hat{\delta}(s)$. As the converter is a switched system, we cannot perfectly describe it with an invariant equation. However, it is possible to obtain an averaged model with a similar enough behavior. To obtain this model, we could use a vector λ associated to $x_e \in X_e$ and obtain the averaged matrices A_λ and B_λ. However, we have observed that this does not generate a good model for all equilibrium points. Therefore, we used the techniques introduced in [14] to obtain a better model. The obtained transfer function is the following.

$$G(s) = \frac{V_s/(LC_o)}{s^2 + sR_o/C_o + 1/(LC_o)} \tag{2.23}$$

These developments conclude all the required modeling for controlling a buck converter, both through min-type and classical controllers.

2.3.2 Boost

The boost converter, also known as step-up, oppositely to the buck, is used when a voltage increase is desirable. To achieve this effect, it uses two operation states. In the first, the source and inductor are short-circuited, generating a high current. After some time, the short circuit is interrupted, changing the power transfer to the output, supplying the load with energy from the source and the inductor. This process regulates power transmission, resulting in a voltage higher than that of the source. The circuit diagram for a synchronous boost converter is presented in Figure 2.1. Our choice for the synchronous topology follows the same reasonings stated in Section 2.3.1.

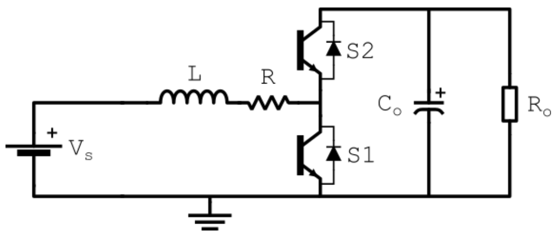

Figure 2.3: Synchronous Boost circuit diagram.

As happens with the buck converter, the presence of these two switches results in four possible combinations. However, one is of no interest because it leaves the output as an open circuit. The other imposes a short-circuit in the capacitor, which is also of not interest. Of the valid remaining states, the first corresponds to the situation where S_1 is active and the second when S_2 is active. To describe this behavior mathematically, we use the following state-space matrices.

$$A_1 = \begin{bmatrix} -R/L & 0 \\ 0 & -1/R_oC_o \end{bmatrix}, \quad A_2 = \begin{bmatrix} -R/L & -1/L \\ 1/C_o & -1/R_oC_o \end{bmatrix}$$

$$B_1 = B_2 = \begin{bmatrix} 1/L \\ 0 \end{bmatrix}$$

Based on this set of matrices, we can obtain the set of attainable equilibrium points X_e given in (2.15). As with the buck converter, to operate the system, min-type strategies require both the knowledge of both variables from the equilibrium point. Instead of working with both variables, we derived an equation to determine the corresponding current to a voltage reference.

$$I_e = \frac{V_s}{2R} \pm \sqrt{\frac{V_s^2}{4R^2} - \frac{V_e^2}{RR_o}}$$

However, the problem with this equation is that there are two possible equilibrium currents for each voltage reference. To overcome this problem, we can discard the highest values, as they result in a much lower efficiency.

$$I_e = \frac{V_s}{2R} - \sqrt{\frac{V_s^2}{4R^2} - \frac{V_e^2}{RR_o}} \tag{2.24}$$

With the same method used to obtain the equation for I_e, it is possible to determine the values of λ that corresponds to a certain equilibrium point.

$$\lambda := \begin{cases} \lambda_1 = \frac{V_s - RI_e}{V_e} \\ \lambda_2 = 1 - \lambda_1 \end{cases} \tag{2.25}$$

These results are illustrated in the graphs of Figure 2.2.

The equations developed until here are already enough to control the converter through min-type strategies. Let us shift the focus to the classical controller. For its control, as will be

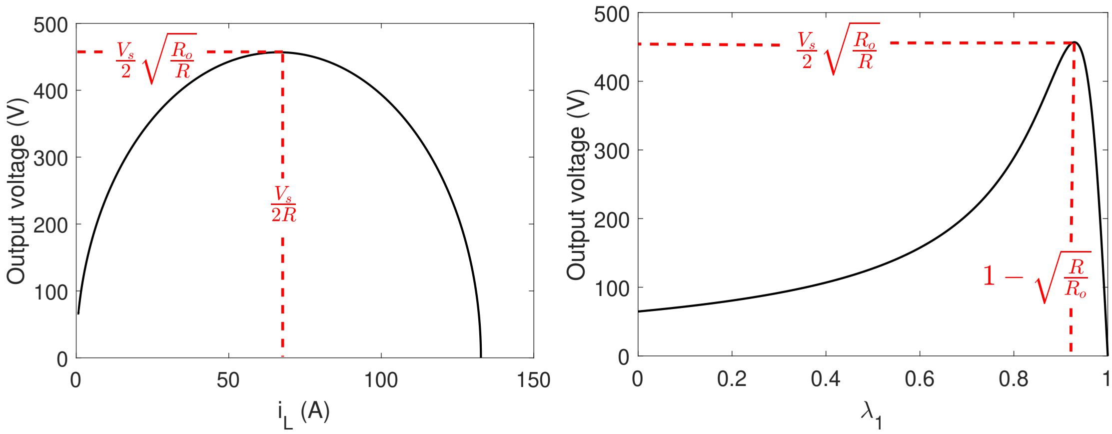

(a) Equilibrium region X_e for the boost converter.

(b) Relation between λ_1 and the equilibrium voltage V_e for the boost converter.

Figure 2.4: Equilibrium region and its relation to λ for the boost converter.

further explained in Chapter 3, we require an LTI model, which we represent as the following transfer function.

$$G(s) = -\frac{V_e^2}{V_s R_o C_o} \frac{s + \frac{1}{L}\left(R - R_o \frac{V_s^2}{V_e^2}\right)}{s^2 + s\left(\frac{R}{L} + \frac{1}{C_o R_o}\right) + \frac{1}{C_o L}\left(\frac{R}{R_o} + \frac{V_s^2}{V_e^2}\right)} \tag{2.26}$$

As this is not the focus of our study and is already a consolidated technique, the mathematical developments to obtain this function are omitted (see [14] for details). Thus we conclude all the required modeling for the control of a boost converter.

2.3.3 Buck-Boost

The buck-boost converter is a versatile combination of both previously presented converters. It is capable of supplying the load with voltages both lower and higher than that of the source. This versatility is achievable through the use of two states. In the first stage, the power source is short-circuited with the inductor, powering it up. The source is then disconnected, and the energy stored in the inductor is transferred to the load. With the increase of the inductor energization time, the output voltage tends to go up. The circuit diagram for a synchronous buck-boost converter is presented in Figure 2.5.

Unlike both previous converters, this topology uses four switches to operate, which allows four state combinations. However, most are not relevant. Considering the sets of switches (S_1, S_2) and (S_3, S_4), any state where both gates of the same set are open or closed is not relevant. From the remaining, only two are of interest in an ordinary operation. The first occurs when

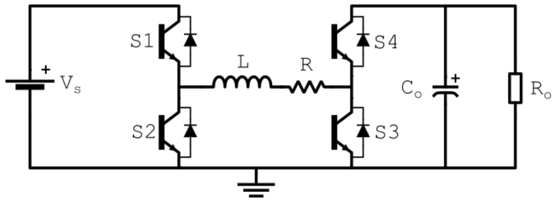

Figure 2.5: Synchronous Buck-Boost circuit diagram.

the active switches are S_1 and S_3, the second when S_2 and S_4 are active. Considering these switched we obtain the following state-space matrices

$$A_1 = \begin{bmatrix} -R/L & 0 \\ 0 & -1/R_oC_o \end{bmatrix} \quad B_1 = \begin{bmatrix} 1/L \\ 0 \end{bmatrix}$$

$$A_2 = \begin{bmatrix} -R/L & -1/L \\ 1/C_o & -1/R_oC_o \end{bmatrix} \quad B_2 = \begin{bmatrix} 0 \\ 0 \end{bmatrix}$$

With the determination of all state-space matrices, it is already possible to determine the equilibrium points and to obtain an equation that relates the equilibrium current with a specific voltage reference, as presented in the sequel

$$I_e = \frac{V_s}{2R} - \sqrt{\frac{V_s^2}{4R^2} - \frac{V_e(V_e + V_s)}{RR_o}} \tag{2.27}$$

Furthermore, in an equivalent manner, it is possible to obtain the set of equations

$$\lambda := \begin{cases} \lambda_1 = \frac{V_e + RI_e}{V_s + V_e} \\ \lambda_2 = 1 - \lambda_1 \end{cases} \tag{2.28}$$

to determine the values of λ from a specific equilibrium point.

Both these results are illustrated in the graphs of Figure 2.6.

We have then concluded the modeling required for the converter operation with min-type controllers. Lastly, let us shift the focus to the classical controller. To its design, a LTI model of the type $G(s) = \hat{V}_o(s)/\hat{\delta}(s)$ is required. Using the techniques from [14], we obtained the equation

$$G(s) = -\frac{V_e^2}{R_oV_s} \frac{Ls + R - \frac{R_oV_s^2}{V_e^2}}{C_oLs^2 + s\left(C_oR + \frac{L}{R_o}\right) + \frac{R}{R_o} + \left(\frac{V_e}{V_e + V_s} - 1\right)^2}$$

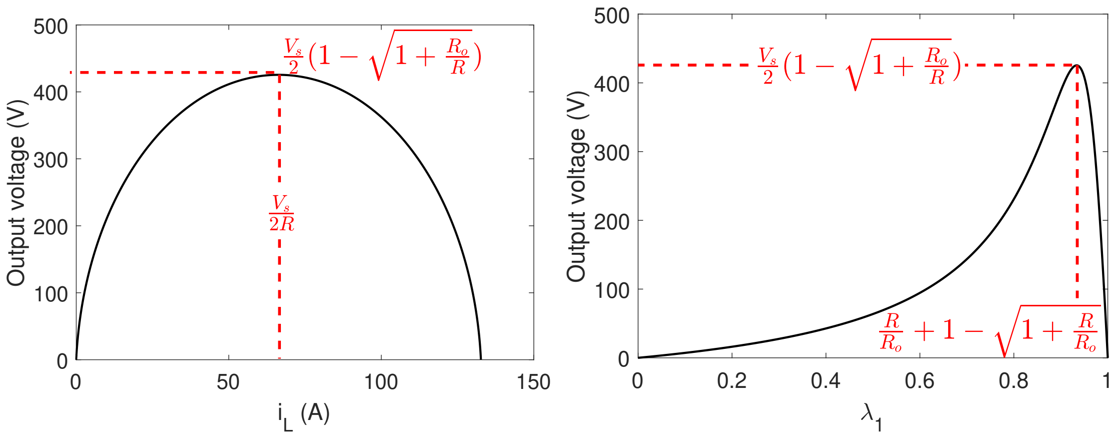

(a) Equilibrium region X_e for the buck-boost converter.

(b) Relation between λ_1 and the equilibrium voltage V_e for the buck-boost converter.

Figure 2.6: Equilibrium region and its relation to λ for the buck-boost converter.

which presents the LTI model in the frequency domain. Note that it depends on the desired output voltage V_e. At this point, we concluded the modeling of the buck-boost converter which will be useful for all types of controllers presented in the next chapter.

2.4 Chapter Considerations

Throughout this chapter, we presented some well-established concepts and equations. Although they are found in the literature, they are essential to the study. The primary focus of the chapter was the modeling of the switched affine systems, more specifically DC-DC converters.

First, we explored the modeling of affine time-invariant systems, both in the continuous and discrete-time domains. These results were then expanded to enable the modeling of switched affine systems. This last modeling was the one used for the mathematical representation of the DC-DC converters. Three different topologies were modeled. The buck, boost, and buck-boost. Other than their model, we also obtained equations that will assist with the control design and its implementation.

With the developments from this chapter, we can already shift the focus to the real contributions of this work, which are the control strategies and the analysis of their applications. In the next chapter, we will explore the control design and present some of our contributions.

Chapter 3

Control Strategies

This chapter presents our main contributions from a theoretical point of view. More specifically, some control strategies capable of stabilizing the DC-DC converters are provided, emphasizing the PWM-based strategy and the min-type switching strategies. The first is used for comparison and is the most common method to operate the converter switches. It uses a classical controller to determine the duty-cycle dynamically. In this case, the control design is based on the LTI model of the converter, which can be obtained by linearizing the system around the desired equilibrium point. The min-type switching strategies are designed, taking into account the original switched affine system without any approximation. More specifically, three min-type switching strategies have been considered. Two of them suppose an arbitrarily high switching frequency. The other, more realistic, considers a sampled-data control strategy and, therefore, a limited frequency. In the literature, most of these methodologies are designed to operate in one specific equilibrium point. Our main contribution is to generalize the techniques based on min-type switching strategies to make them able to operate under changes in the equilibrium points and load variations without the need for redesign. During the practical implementations, these changes and variations are expected. Taking them into account during the control design is undoubtedly a relevant improvement. A correction method is also proposed to assure zero-error operation.

3.1 PWM-based strategies

The use of a PWM signal to operate switched DC-DC converters is very common [21, 24]. It enables the adoption of classical controllers to dynamically adjust its duty cycle, making the control design a more amenable task. The method relies on two main components: a classical controller and a PWM signal generator. Usually, the voltage error is the input to the controller. Its output supplies the PWM signal generator with an appropriate duty cycle. The duty cycle is closely related to the vector $\lambda \in \Lambda$. Indeed, by varying the duty-cycle, we change the convex combination of subsystems, consequently changing the equilibrium point. Figure 3.1 presents the control scheme.

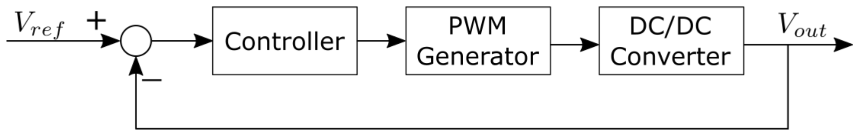

Figure 3.1: Block diagram of an output feedback control.

Several classical controllers can be adopted in this situation, such as Proportional-Integral-Derivative (PID), Lead-Lag, and Cascade Lead. They all have their advantages and disadvantages and may result in a better or worst performance for each converter topology and application. However, it is not the objective of this study to analyze all of them. Therefore, we focus only on the Proportional-Integral, which is one of the most common.

A PI controller can be represented considering a continuous-time model in the Laplace domain through the transfer function

$$C(s) = \frac{\hat{\delta}(s)}{\hat{e}(s)} = k_p + k_i \frac{1}{s} \tag{3.1}$$

where e and δ denote the voltage error and the duty-cycle, respectively.

Multiple techniques can be used to design $C(s)$ and choose its constants (k_p and k_i). However, we will focus on the method usually applied in power electronics applications. In this method, the designer chooses an adequate phase margin and the crossover frequency for the controlled system $C(s)G(s)$, where $G(s)$ denotes the averaged model of the converter. Procedure 3.1 presents the required steps to design the controller. For a deeper understanding, see [14].

Procedure 3.1: Design of a PI controller through phase and gain margins

Step 1: Choose an adequate crossover frequency ω_0 and phase margin ϕ_0.

Step 2: Determine the phase of $G(s)$ at the frequency ω_0.

$$\phi_G = \angle G(j\omega_0)$$

Step 3: Determine the phase margin F_m that results in the phase ϕ_0.

$$F_m = \phi_0 - \phi_G - \pi/2$$

Step 4: $T_i = \tan(F_m)/\omega_0$

Step 5: Calculate the proportional gain of the controller.

$$k_p = \frac{1}{\|G(j\omega_0)\|\sqrt{1 + (T_i\omega_0)^2}}$$

Step 6: Calculate the integral gain of the controller.

$$k_i = \frac{k_p}{T_i}$$

By following these steps, the designer can obtain the transfer function of the PI controller in the continuous-time domain. However, for practical implementations, a discrete-time controller is more suitable because control boards are digital systems with time constraints.

To obtain a discrete representation of the controller, the Forward Euler approximation can be used. This transform is capable of converting a transfer function $F(s)$ from the Laplace domain to $F(z)$ in the Z-domain. In this transform, the relation between both domains is given by

$$s = \frac{z - 1}{T_s} \tag{3.2}$$

where T_s denotes the discretization period.

Using this relation, a function $C(z)$ can be easily determined.

$$C(z) = \frac{\hat{\delta}(z)}{\hat{e}(z)} = k_p + k_i \frac{T_s}{z - 1} \tag{3.3}$$

Finally, the function can be taken from the Z-domain to the discrete-time domain, by remembering that $z^{-1}F(z) = f[k-1]$

$$\delta[k] = k_p e[k] + (k_i T_s - k_p) e[k-1] + \delta[k-1] \tag{3.4}$$

which is ready to be implemented.

3.2 Robust Min-Type Switching Strategies

An important characteristic of the min-type switching strategies is that they consider the original switched affine system without approximation.

In this section, three min-type switching control strategies are taken into account. Two of them were borrowed from [10] and do not consider any limitation on the switching frequency. Their importance in this dissertation stems from the fact that they have been used as a basis for generalizations in several works, see the recent references[4, 28, 33, 34]. However, both techniques suppose an infinite switching frequency to guarantee asymptotic stability, which is not possible in practical applications due to the physical limitations of digital circuits.

To circumvent this problem, the authors in [9, 26, 28] have proposed conditions for the control design of sampled-data switching strategies allowing to impose a bound on the switching frequency. The references [26, 28] impose a dwell-time to the switching function. Meanwhile, [9] adopts a specific discrete-time system as a basis to obtain the control design. It is important to remark that asymptotic stability cannot be assured when the switching frequency is limited. In this case, the stability is practical. It differs from asymptotic stability because it does not attain an equilibrium point but a region containing this point.

Unfortunately, a great inconvenience from these control methodologies and others from the literature is that they are not robust to changes in the equilibrium points and load variations. These two phenomena are prevalent in the practical applications of power electronics. Their disregard can limit the use of these control methodologies. Due to the importance of considering load variations, references [28, 30] have proposed an alternative solution to deal with this problem through an external control loop. However, this solution does not have theoretical proof of stability.

In this section, we have generalized the stability conditions of [10] and [9] to make them able to operate under changes in the equilibrium points and load variations without the need for a redesign. In our opinion, this simple generalization is important mainly in the point of view of practical implementations.

As it will be evident in the sequel, we separated the min-type control strategies presented here as sampled and non-sampled ones. The non-sampled rules are designed for the continuous-time model and derived from [10]. In contrast, the sampled one originates from a specific discrete-time model and is generalized from [9].

3.2.1 Non-Sampled controllers

In this subsection, we have taken into account two min-type switching strategies borrowed from [10] and based on the simple quadratic Lyapunov function

$$v(x) = (x - x_e)' P(x - x_e) \tag{3.5}$$

with $P > 0$. Defining a controlled output for the system (2.9) as being

$$z = C_\sigma(x - x_e) \tag{3.6}$$

both state-dependent switching rules have been designed in order to assure global asymptotic stability of the equilibrium point $x_e \in X_e$ and the cost

$$\int_0^\infty (z - C_\sigma x_e)'(z - C_\sigma x_e)dt < (x_0 - x_e)' P(x_0 - x_e) \tag{3.7}$$

Ideally, the goal is to design $\sigma(x(t))$ by minimizing the left side of (3.7). However, due to the nonlinear and time-varying nature of the switching function, this task is too hard to accomplish. Therefore, the aim is to minimize the right side of (3.7), obtaining a suitable guaranteed cost. As it will be clear in the sequel, the control design of these non-sampled switching strategies requires an infinite switching frequency, making the rules suitable for many applications in power electronics where the frequency can be sufficiently high.

The first rule presented here derives from Theorem 2 of [10]. This switching function is denoted as Quadratic Non-Sampled (QNS) controller and is very conservative since it requires that all subsystems be quadratically stable as a necessary condition for stability. Notice that it is not enough to assure the stability of all subsystems, which is relatively simple for several real systems, including the converters considered in this thesis. Besides being all stable, they need to share the same Lyapunov matrix, which restricts the range of applicability of this methodology. On the other hand, it has the advantage of being robust to changes in the equilibrium points. However, it is not robust to changes in the output load, which alters the system model.

To overcome this limitation, we have proposed an improvement in the control design of [10] generalizing the conditions to cope with this previously unhandled situation. Let us define the set S_R containing all η output resistances for which stability is desired as being

$$S_R = \{R_o^1, \cdots, R_o^\eta\} \tag{3.8}$$

The A_i matrix is then represented as a function of the output resistance, which together with the set (3.8) yields $A_i(R_o^k) = A_i^k,\ \forall k \in \{1, \cdots, \eta\}$ with $R_o^k \in S_R$. In Chapter 4, this matrix will be handled to make the switching rule more efficient in terms of numerical complexity during the implementation. To allow the operation with the extended model, the load must be inside the set S_R and be identified during the converter operation. This determination can be done through the measurement or estimation of the output resistance. As a consequence of this extended, the set of equilibrium points is changed as well. Each value of A_k results in a different equilibrium region X_e^k summing a total of η different sets X_e^k. The next theorem presents the control design conditions.

Theorem 1 *Consider the switched affine system* (2.9) *with the controlled output* (3.6) *and choose an equilibrium point* $x_e^k \in X_e^k$. *If there exists* $P > 0$ *capable of solving the complex optimization problem*

$$P = \arg \inf_{P>0} \mathrm{Tr}(P) \tag{3.9}$$

subject to the LMIs

$$A_i^{k\prime} P + P A_i^k + C_i' C_i < 0,\ \ i \in \mathbb{K} \text{ and } k \in \{1, \cdots, \eta\} \tag{3.10}$$

then the state-dependent switching function

$$\sigma(x) = \arg \min_{i \in \mathbb{K}} (x - x_e^k)' P (A_i^k x_e^k + B_i u) \tag{3.11}$$

assures global asymptotic stability for any $x_e^k \in X_e^k$, *with* $k \in \{1, \cdots, \eta\}$. *Consequently, the system is also robust regarding load variations for any* $R_o \in S_R$, *considering that the load change is sufficiently slow.*

Proof 1 *The proof follows the same pattern to the one presented in the Theorem 2 of [10], therefore it is simplified here. Consider the quadratic Lyapunov function* (3.5) *and define* $\xi = x - x_e$ *and*

$C'_\sigma C_\sigma = Q_\sigma$. Adopting the switching rule (3.11)*, we have*

$$\begin{aligned}
\dot{v}(\xi) &= \dot{\xi}' P\xi + \xi' P\dot{\xi} \\
&= 2\xi' P(A^k_\sigma x + B_\sigma u) \\
&= 2\xi' P(A^k_\sigma x^k_e + B_\sigma u) + \xi'(A'^k_\sigma P + PA^k_\sigma)\xi \\
&= \min_{i\in\mathbb{K}}(2\xi' P(A^k_i x^k_e + B_i u)) + \xi'(A'^k_\sigma P + PA^k_\sigma)\xi \\
&< \min_{\lambda\in\Lambda}\max_{k\in\{1,\cdots,\eta\}}(2\xi' P(A^k_\lambda x^k_e + B_\lambda u)) - \xi' Q_\sigma \xi \\
&\leq \max_{k\in\{1,\cdots,\eta\}}(2\xi' P(A^k_\lambda x^k_e + B_\lambda u)) - \xi' Q_\sigma \xi \\
&< -\xi' Q_\sigma \xi
\end{aligned} \tag{3.12}$$

where the first inequality comes from (3.10)*, the second is due to a known property of the minimum operator, and the last one is a consequence from the fact that $x^k_e \in X^k_e$ which imposes $A^k_\lambda x_e + B_\lambda u = 0$.*

As it has been already mentioned, this theorem requires that matrices A^k_i be quadratically stable for all $i \in \mathbb{K}$ and $k \in \{1, \cdots, \eta\}$ making this result very conservative at the cost of being robust concerning changes in x^k_e. However, the vast majority of applications operate the converter within a limited range of equilibrium points, requiring only a subset of X^k_e for each $k \in \{1, \cdots, \eta\}$. Therefore, a less conservative control strategy based on Theorem 1 of [10] can be obtained focused on the desired range of operation.

The main difference between this rule proposed in [10] and the QNS controller is that it assures asymptotic stability only for a specific equilibrium, defined during the control design. This aspect requires redesign whenever the converter needs to change its output voltage. To circumvent this problem, we propose a simple generalization. Instead of making the control design considering a single equilibrium point, we now design the controller to operate with M distinct voltages. To do this, for each output resistance R^k_o, $\forall k \in \{1, \cdots, \eta\}$, we define a set of M equilibrium points of interest

$$S^k_{ec} = \{x^{k,1}_e, \cdots, x^{k,M}_e\} \tag{3.13}$$

such that $S^k_{ec} \subset X^k_e$ and the associated vector is $\lambda(x^{k,j}_e) = \lambda^{k,j} \in \Lambda$, $\forall j \in \{1, \cdots, M\}$. The next theorem presents the stability conditions.

Theorem 2 *Consider the switched affine system* (2.9) *with the controlled output* (3.6) *and choose an equilibrium point $x_e = x^{k,j}_e \in S^k_{ec}$ with its associated vector $\lambda = \lambda(x^{k,j}_e) = \lambda^{k,j} \in \Lambda$ for some*

$j \in \{1, \cdots, M\}$ and $k \in \{1, \cdots, \eta\}$. If there exists a matrix $P > 0$ satisfying the LMIs

$$A'_{\lambda^{k,j}} P + P A_{\lambda^{k,j}} + Q_{\lambda^{k,j}} < 0 \tag{3.14}$$

for all $j \in \{1, \cdots, M\}$ and $k \in \{1, \cdots, \eta\}$ where

$$A_{\lambda^{k,j}} = \sum_{i=1}^{N} \lambda_i^{k,j} A_i^k, \; Q_{\lambda^{k,j}} = \sum_{i=1}^{N} \lambda_i^{k,j} C_i' C_i, \tag{3.15}$$

then the state-dependent switching function

$$\sigma(x) = \arg\min_{i \in \mathbb{K}} (x - x_e^{k,j})' \Big(2P(A_i^k x + b_i) + C_i' C_i (x - x_e^{k,j}) \Big) \tag{3.16}$$

assures the global asymptotic stability of any equilibrium point $x_e = x_e^{k,j} \in S_{ec}^k$, $j \in \{1, \cdots, M\}$, $k \in \{1, \cdots, \eta\}$ and the guaranteed cost

$$\int_0^{\infty} z' z dt < (x_0 - x_e^{k,j})' P (x_0 - x_e^{k,j}) \tag{3.17}$$

is satisfied.

Proof 2 *The proof is direct and follows the same reasoning of the one in Theorem 1 of [10] and will be presented here in general lines. Choosing an equilibrium point $x_e = x_e^{k,j} \in S_{ec}^k$, defining $\xi = x - x_e$, and adopting the switching function* (3.16)*, the time-derivative of the Lyapunov function under an arbitrary trajectory of* (2.9) *provides*

$$\begin{aligned}
\dot{v}(\xi) &= \xi' \Big(2P(A_\sigma^k \xi + A_\sigma^k x_e + B_\sigma u) + C_\sigma' C_\sigma \xi \Big) - z_e' z_e \\
&= \min_{i \in \mathbb{K}} \xi' \Big(2P(A_i^k \xi + A_i^k x_e + B_i u) + C_i' C_i \xi \Big) - z_e' z_e \\
&\leq \max_{k \in \{1, \cdots, \eta\}} \max_{j \in \{1, \cdots, M\}} \xi' \Big(2P(A_{\lambda^{k,j}} \xi + A_{\lambda^{k,j}} x_e + B_{\lambda^{k,j}} u) + Q_{\lambda^{k,j}} \xi \Big) - z_e' z_e \\
&< -z_e' z_e
\end{aligned} \tag{3.18}$$

where the second equality comes from the switching function, the first inequality is due to the fact that

$$\min_{i\in\mathbb{K}} \xi'(2P(A_i^k x + B_i u) + C_i' C_i \xi) = \min_{\lambda^{k,j}\in\Lambda} \xi'(2P(A_{\lambda^{k,j}} x + B_{\lambda^{k,j}} u) + Q_{\lambda^{k,j}} \xi)$$
$$\leq \max_{k\in\{1,\cdots,\eta\}} \max_{j\in\{1,\cdots,M\}} \xi' \left(2P(A^k_{\lambda^{k,j}} x + B_{\lambda^{kj}} u) + Q_{\lambda^{k,j}} \xi \right)$$

and the last inequality comes from the validity of (3.14) *and is a consequence of the fact that* $x_e = x_e^{k,j} \in X_e^k$ *which implies that* $A_{\lambda^{k,j}} x_e + B_{\lambda^{k,j}} = 0,\ \forall j \in \{1, \cdots, M\},\ k \in \{1, \cdots, \eta\}$. *The guaranteed cost is obtained directly by integrating both sides of* (3.18) *from* $t = 0$ *to* $t \longrightarrow \infty$ *and using the fact that* $\lim_{t\to\infty} v(x(t)) = 0$ *due to the asymptotic stability of the system.*

We can denote the control strategy proposed in this theorem as Robust Non-Sampled (RNS) controller. It is a min-type controller robust to changes in both the output load and the equilibrium points. As it will be seen further, this rule already presents promising results; however, it does not solve all the problems. It still requires an arbitrarily fast switching frequency.

To avoid this problem, reference [9] has proposed a sampled-data switching rule whose control design considers a specific discrete-time model. The following section generalizes this result to make it robust concerning the two studied situations.

3.2.2 Sampled controllers

The development of sampled min-type controllers was motivated by the infinity switching frequency problem of the non-sampled controllers. Studies such as [19, 26, 28] tried to circumvent this problem by imposing time constraints and assuring practical stability. Another approach was through the use of limit-cycles (see [6, 12]). They enable the converter to follow a determined periodic solution of the switched affine system.

Using the discrete-time model obtained by discretization of the continuous-time counterpart, which has been presented in (2.17) with matrices (2.18), the switching frequency is naturally limited, making the controller suitable for practical implementation. It is important to remember that, in this case, the switching rule satisfies a time constraint being modeled as in (2.16).

The controller proposed here is derived from [9] and is based on the following general quadratic Lyapunov function

$$v(\xi) = \begin{bmatrix} 1 \\ \xi \end{bmatrix}' \begin{bmatrix} h'P^{-1}h & h' \\ h & P \end{bmatrix} \begin{bmatrix} 1 \\ \xi \end{bmatrix} \tag{3.19}$$

with $h \in \mathbb{R}^n$, $x - y_e = \xi \in R^{n \times 1}$, and $0 < P \in \mathbb{R}^{n \times n}$ to be determined. The set of equilibrium points Y_e was defined in (2.19).

As the controllers presented in [10], the sampled controller of [9] is also not robust to changes in the equilibrium points nor the output load. Therefore, the same generalization proposed before is adopted in this case. The problem of robustness regarding load variations can be circumvented by using the set $S_R = \{R_o^1, \cdots, R_o^\eta\}$.

We can then determine η models for the converter, one for each output load. In this case, the matrices are dependent on the output resistance being denoted as $A_i^k = A_i(R_o^k)$, $F_i^k = F_i(R_o^k)$ and $G_i^k = G_i(R_o^k)$, where $k \in \{1, \cdots, \eta\}$ and $R_o^k \in S_R$. Related to the robustness with respect to changes in the equilibrium points, the same method used with the RNS controller can be applied. Again, let us define a set of M equilibrium points of interest given by

$$S_{ed}^k = \{y_e^{k,1}, \cdots, y_e^{k,M}\} \tag{3.20}$$

with the associated vector $\lambda(y_e^{k,j}) = \lambda^{k,j} \in \Lambda$, $\forall j \in \{1, \cdots, M\}$. The next theorem presents this result.

Theorem 3 *Consider the switched affine system* (2.3) *with the controlled output* (3.6) *with* $C_i = C$, $\forall i \in \mathbb{K}$ *and choose an equilibrium point* $y_e = y_e^{k,j} \in S_{ed}^k$ *with its associated vector* $\lambda = \lambda(y_e^{k,j}) \in \Lambda$ *for some* $j \in \{1, \cdots, M\}$ *and* $k \in \{1, \cdots, \eta\}$. *Defining,* $\ell_i^{k,j} = (F_i^k - I)y_e^{k,j} + G_i^k u$, $\forall i \in \mathbb{K}$, *if there exist* $P > 0$ *and a scalar* $\gamma > 0$ *solution of the following convex optimization problem*

$$\max_{P>0, \gamma>0} \gamma \tag{3.21}$$

subject to

$$\sum_{i \in \mathbb{K}} \lambda_i^{k,j} F_i^{k\prime} P F_i^k - P < -\gamma C' C, \ \sum_{i \in \mathbb{K}} \lambda_i^{k,j} \ell_i^{k,j\prime} P \ell_i^{k,j} < 1 \tag{3.22}$$

for all $j \in \{1, \cdots, M\}$ *and* $k \in \{1, \cdots, \eta\}$*, then the state-dependent switching function*

$$\sigma(x) = \arg\min_{i \in \mathbb{K}} v(F_i^k x + G_i^k u) \tag{3.23}$$

with $v(x)$ *completely defined by*

$$h^{k,j} = (I - F'_{\lambda^{k,j}})^{-1} \Big(\sum_{i \in \mathbb{K}} \lambda_i^{k,j} F_i^{k\prime} P \ell_i^{k,j} \Big) \tag{3.24}$$

assures the global practical stability of any equilibrium point $y_e = y_e^{k,j} \in S_{ed}^k$, $j \in \{1, \cdots, M\}$, $k \in \{1, \cdots, \eta\}$ *and that the controlled output* z *converges to the ball*

$$\mathcal{B} = \{z \in \mathbb{R}^{n_z} \;\; : \;\; z'z \leq \gamma^{-1}\} \tag{3.25}$$

Proof 3 *The proof follows the same pattern of the one in [9], with* $\gamma C'C \longrightarrow W$ *and adapted to hold robustly for different equilibrium points* $y_e^{kj} \in S_{ed}^k$ *and output loads* $R_o \in S_R$*, therefore, it will be omitted.*

Let us denote the min-type strategy presented in Theorem 3 as Robust Sampled (RS) controller. It is now robust regarding changes in the equilibrium point and output load. As mentioned in [9], to take into account the sampled-data switching function, the following additional constraints

$$\gamma(x_e^{k,j} - y_e^{k,j})' C' C (x_e^{k,j} - y_e^{k,j}) < 1, \; j \in \{1, \cdots, M\}, \; k \in \{1, \cdots, \eta\} \tag{3.26}$$

must be included in Theorem 3 to assure that the corresponding $x_e^{k,j}$ of the continuous-time system is inside the set of attraction. Notice that for evaluating the switching function $\sigma(x)$, the vector h must be calculated during operation, as it depends on the equilibrium point.

3.3 Steady-State Correction

Despite the theoretical advantages of the min-type switching strategies, they suffer from the inconvenience of not always operating at zero error on practical implementations. This nuisance occurs due to some reasons. The design of non-sampled switching strategies considers an arbitrarily high frequency, impossible to obtain in practical applications due to physical limitations. This limitation motivated the development of sampled switching rules, which already consider the time constraints from digital implementations during the control design. Although this change dramatically improves the steady-state response of the converter, it does not exempt these strategies from the existence of a steady-state error, as they operate with assured practical, not asymptotic, stability.

Divergences between the model and the real system may also induce voltage errors. These differences may be originated from bad modeling, not considered behaviors, or merely a variation in the output load or the input voltage. The error caused by these model uncertainties is inconvenient for many applications that require a robust converter capable of operating at multiple conditions. The standard PWM-based methods usually rely on an integrator to compensate for any unmodeled behavior. To mimic this with the min-type strategies, some studies, such as [10, 28], proposed an external control loop.

This external control loop operates based on the voltage error. It is responsible for adjusting the equilibrium point, forcing the system to operate at the desired voltage. In [28], this loop consists of a PI controller, which uses the steady-state error to adjust the equilibrium voltage V_e in order to make it attain as near as possible the desired reference voltage. Based on this value, the system then calculates the corresponding equilibrium current. In [15], the equilibrium voltage is equal to the reference, while the loop adjusts the equilibrium current. In our method, a PI is still responsible for the correction. However, we have added a feed-forward loop where the controller is only used to correct part of the equilibrium voltage, as it will be clear afterward.

Inspired by previous studies, we proposed two steady-state correction techniques. The first method is inspired by the one from [28], and its diagram is presented in Figure 3.2. However, differently from this reference, we have added a feed-forward loop of the reference voltage, using the PI only to correct the equilibrium point. With this simple change, we hope to improve the transient response significantly. It also allowed us to enable or disable the PI controller at any instant during the operation.

Inspired by [15], we have also proposed a second correction method whose diagram is presented in Figure 3.3. The original method from [15] used an integrator to update the equilibrium current. We now propose the replacement of the integrator by a PI controller. The problem with the previous method is its delayed response. For example, in an abrupt load change, the integrator takes some time to respond to the voltage error, enabling the converter to reach undesirable values. Also, without the proportional component in the controller, the

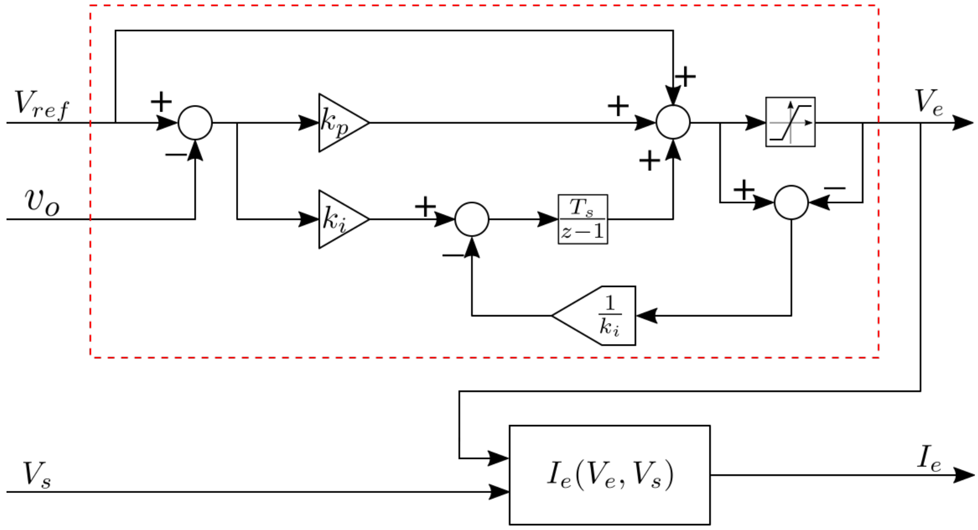

Figure 3.2: Correction method for the equilibrium point's output voltage.

system may perceive some undesirable oscillations. To mitigate the risks, we replaced the integrator with a PI controller. The designer has much more control over the behavior of the system.

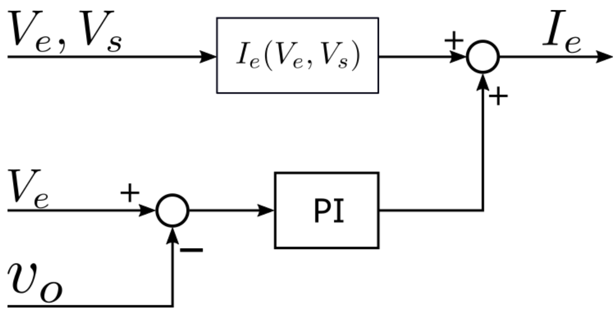

Figure 3.3: Correction method for the equilibrium point's inductor current.

By applying any of these methods, the zero-error operation is already possible. However, these techniques can be even further improved as the objective is to maintain the mean voltage at the desired reference. It is not interesting to use the online value to calculate the voltage error. Instead, a Low Pass Filter (LPF) can obtain the mean value, which is more appropriate for error calculation. Also, there is no need to correct the equilibrium at every switching. By not calculating a new equilibrium on every control loop, we allow the converter to adapt to a value before deciding on a new one. With these modifications, we can mitigate undesirable oscillations, which could be caused by the voltage ripple and measurement noises.

It is easy to notice that an external loop would impact the steady-state and step response. This interference in the transient would negatively affect the expected behavior of a min-type controlled converter. Therefore, the ability to know what is the best time to connect the correction method is essential. It allows us to make its activation after the transient response, thus avoiding any impact during voltage steps. An algorithm to decide when the external loop must be activated is presented in Figure 3.4.

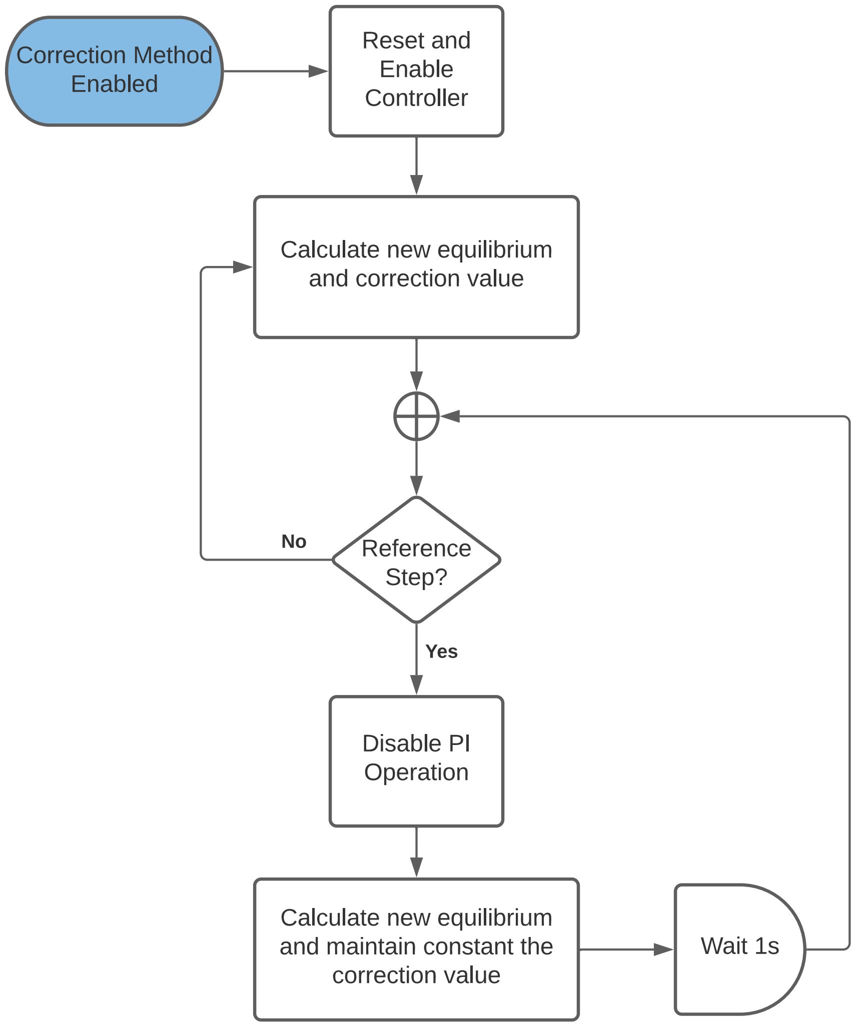

Figure 3.4: Algorithm to engage or disengage the steady state correction mechanism.

Through this algorithm, whenever the system receives a voltage reference step, the correction method is paused by supplying the PI controller with a null error. Notice that the integrator is not taken to zero in these cases, resulting in a smoother transient. Another interesting aspect of this algorithm is that the external loop keeps working when the voltage reference increases gradually following a ramp signal. In this scenario, the correction methods enable the converter to follow the ramp with zero error, further demonstrated.

3.4 Chapter Considerations

In this chapter, we presented the design methodology of four different controllers. Firstly, the classical approach characterized by PWM-based control techniques was reviewed. Although PWM-based controllers are not the focus of this study, this classical method is essential to be used as a basis for comparisons with the novel min-type switching methodologies.

Three different min-type controllers were presented and denoted as Quadratic Non-Sampled (QNS), Robust Non-Sampled (RNS), and Robust Sampled (RS) controllers. Two of them have been developed, taking into account the system in the continuous-time domain. They suffer from the inconvenience of requiring an infinite switching frequency. To circumvent this problem, the other controller has been designed for the system in the discrete-time domain. We have generalized all these proposals to take into account robustness concerning changes in the equilibrium points and load variations, which are two situations very common in practical implementations of the power electronics domain. Moreover, we have proposed two corrections methods for adjusting the steady-state response. The next chapter uses the theoretical results presented here to control the DC-DC converters studied in Chapter 2.

Chapter 4

Experimental Results

In previous chapters, we have presented the converters modeling and the control strategies of interest. Thus, this chapter aims to analyze several aspects of the practical implementation of these control strategies for DC-DC power converters. This analysis has not been made in the literature to date. Its importance comes from the fact that it allows the designers to decide if the min-type switching strategies are good alternatives to classical methodologies.

4.1 Converter Design

For the experimental converter, the option was for a versatile topology. To avoid a different build for all three converters, we chose to build only one converter with the synchronous buck-boost topology. With this configuration, just by changing the operation of the switches, the converter can work as a buck, boost, or buck-boost. Figure 4.1 shows the resulting power circuit.

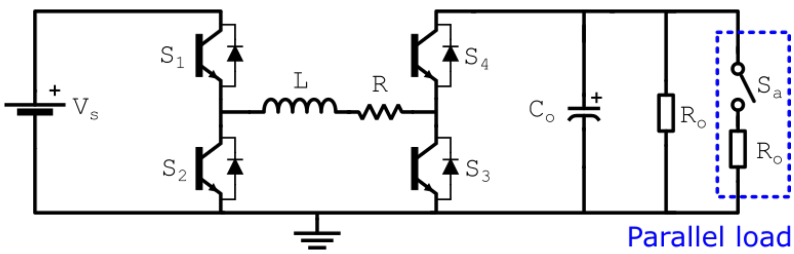

Figure 4.1: Experimental converter circuit diagram.

For the converter to operate as a buck, only the switches (S_1, S_2) are used, meanwhile S_4 is kept conducting and S_3 open. This configuration results in a circuit very similar to the one observed in Chapter 2, except the diode from switch S_3. However, during a regular operation, the diode will not conduct, resulting in an equal behavior.

For the boost configuration, we designed a startup algorithm. When the boost topology is selected, the converter is adjusted to the buck mode. When it is in this mode, the voltage increases gradually, powering up the capacitor until it reaches the maximum voltage, which is the instant when buck operation ceases. The boost is then activated and left on standby at its minimum voltage. This startup avoids the short circuit of the capacitor and the consequent current peak. After this startup, the converter can operate normally by switching the pair (S_3, S_4). In this configuration, S_1 can always be kept conducting, and S_2 always open, resulting in a circuit equivalent to the one observed on Chapter 2.

Lastly, to result in the Buck-Boost operation, we can use all four switches, as presented in Chapter 2.

Notice that the proposed circuit also has an additional parallel load of the same value as R_o. The switch S_a controls its activation. During the regular operation, S_a is kept open. However, by closing the switch S_a, a load step test can be made, enabling the evaluation of the converter performance during load variations.

With the presented topologies, the components were determined. We built a low-power converter with a maximum power output of approximately $300\,W$ for simplicity purposes. The components values are provided in Table 4.1.

Table 4.1: Parameters from the Converter Control Simulation

Parameter	Symbol	Value
Input Voltage (V)	V_s	65
Coil Inductance (mH)	L	1.981
Coil Resistance (Ω)	R	0.49
Output Capacitance (μF)	C_o	2250
Load Resistance (Ω)	R_o	96.8

4.1.1 Simulation

For security purposes and to avoid rework, a simulation model was created before the physical build of the converter. This simulation facilitates the identification of possible mistakes and improvement opportunities during the design step. Another significant advantage is the prior identification of possible operating limits, which served as a guideline for the calibration of the sensors. We developed this model in the *Simulink* software from Matlab. See its main aspects in Figure 4.2.

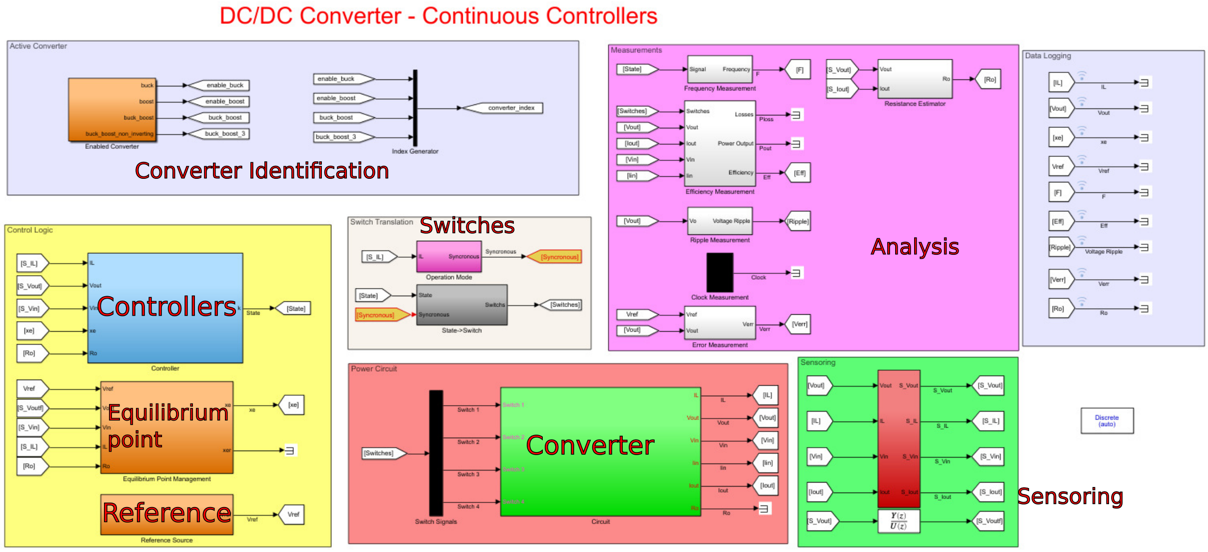

Figure 4.2: Simulink computational model of the converter.

The simulation was made to be as much similar as possible to the real converter. The circuit topology used is equal to the one proposed in (4.1). The switches are also IGBTs with anti-parallel diodes, and the gates' dead-time is also considered. The sensor measurements are sampled at a rate equal to that expected on the real converter.

The simulation works as follows. At an initial moment, the voltage reference is generated, and its value is used to determine the equilibrium point. If a steady-state correction method is active, this point is altered in the orange block of Figure 4.2 responsible for managing the equilibrium point. The equilibrium point and the circuit measurements are then supplied to the converter, which determines the appropriate subsystem to be active at each instant of time. This signal is then delayed to compensate for the computational time. The delayed state information is then translated as signals for all switches, which will suffer from further delays, to simulate the gate driver dead-time. They are then operated if necessary. In the simulation, it is also possible to measure values such as the switching frequency, perceived output load, steady-state error, and ripple.

Through this mathematical model, we tuned the controllers to respect the operation range of the physical converters.

4.1.2 Converter Build

After the initial simulations, we built an experimental converter. In this section, we will approach its most relevant aspects and present the experimental results.

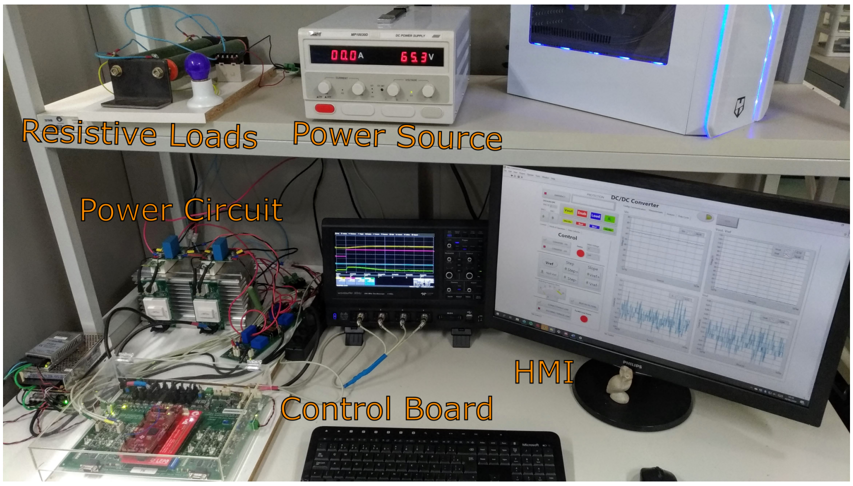

Figure 4.3: Experimental converter build.

For the switches $\{S1, \cdots, S4\}$, we used IGBTs with anti-parallel diodes, as was shown in Figure 4.1. The IGBTs are SKM150GB12T4 from Semikron and are operated through gate drivers SKHI 21A.

A total of four Hall effect sensors are used. The measured variables are the input and output voltages (LEM LV 20-P) and the inductor and output currents (LEM LA 55-P). Of these, the only measurement that is not directly used during the control design is the output current. However, it can be helpful for the estimation of the output load.

To enable a broader range of tests and be capable of online changing the converter and its controller, we used the control board TMS320F28379D from Texas Instruments. Its processor can operate at a frequency of up to 200 MHz and has two cores and a floating processing unit of 32 bits. These aspects significantly increase the performance, resulting in a minor delay between measurement and control actions. The multiple cores also allow us to dedicate a core for the control routines. Therefore the implementation of communications and other less critical behaviors can be made in the other core without impacting the control performance.

We also built a Human Machine Interface (HMI) with the LabView software to operate the converter. Using this interface, the operator can choose the voltage reference and select the converters and the control strategy to be adopted through it. It also enables the operator to monitor all measured variables, the voltage ripple, switching frequency, and the duty cycle.

4.1.3 Control Design

Before delving into the control design, some necessary definitions are in order. Let us define switching frequency as the frequency of the PWM signal, commutation frequency as the number of commutations per second, and control frequency as the rate at which the controller is executed. One crucial aspect of the control implementation is the definition of its control frequency. The used gates have a rated maximum switching frequency of 20 kHz. Therefore, the chosen execution period must be compatible with this value. We opted to operate the switches at their maximum possible frequency, and, therefore, the chosen PWM frequency was 20 kHz.

Meanwhile, the min-type switching strategies will operate at a maximum commutation frequency of 40 kHz. This higher value for min-type controllers is because two commutations occur during a PWM period. Hence, a switching frequency of 20 kHz is equivalent to a commutation frequency of 40 kHz. For the min-type switching strategies, the control frequency is also 40 kHz, while, for the PWM-based ones, this value is equal to 20 kHz.

The required discretizations are made following the control frequency. For PWM-based strategies, the discretization period is $T_s = 50\mu$s and for the min-type controllers the period is of $T_s = 25\mu$s. Notice that for the PWM-based controllers, the control frequency is equal to that of the PWM signal.

Using the continuous-time transfer function $G(s)$ of each converter presented in Chapter 2, we can design the PWM-based PI controller. By choosing good gain and phase margins for each converter, we can follow the Procedure 3.1 and easily determine the controller. Table 4.2 contains the margins used and the determined controller for each converter. Using the values of k_p and k_i, the control can be easily implemented through (3.4).

Table 4.2: Output feedback PI Controllers

Variable	Buck	Boost	Buck-Boost
Design Parameters			
ω_0 (rad/s)	28	279	190
θ_0 (°)	13	40.1	60
Control Variables			
k_p	0.00364	0.00312	0.00283
k_i	2.35	1.05	0.312

For the min-type switching strategies, the control problem consists of determining the matrix $P > 0$ for the Lyapunov function, subject to the constraints presented throughout Section 3.2. For the design, the matrix products $C_i'C_i$ must be provided. They are important to assure guaranteed cost in Theorems 1, 2 and 3. For simplicity purposes, we consider the same controlled output to all subsystems, therefore

$$C_i'C_i = C'C, \ \forall i \in \mathbb{K} \tag{4.1}$$

we have chosen different values for each converter to obtain a rapid response while attaining the current limitation of 20 A, imposed by the sensors. We also need to provide the vector S_R containing all the output loads to be considered during the control design. For this application, we considered

$$S_R = \{0.1R_o, 0.2R_o, \cdots, R_o, \cdots, 2R_o\} \tag{4.2}$$

Therefore, we have $\eta = 20$ different models. This high number is not a problem for the control design and simulations. However, it is not practical to have 20 different models on the microcontroller. To overcome this inconvenience, we opted for an online model calculation.

This was achieved by representing matrix $A_i = \{a_i(m,n)\} \in \mathbb{R}^{2\times 2}$ as a function of the output load. To do this, we factored A_i into two new matrices, $A_i^0 = \{a_i^0(m,n)\} \in \mathbb{R}^{2\times 2}$ and $A_i^R = \{a_i^R(m,n)\} \in \mathbb{R}^{2\times 2}$. The elements of the matrix A_i^0 are defined as $a_i^0(m,n) = a_i(m,n)$ when $a_i(m,n)$ is independent of R_o, else $a_i^0(m,n) = 0$. The elements of the matrix A_i^R are given by $a_i^R(m,n) = 0$ when $a_i(m,n)$ is independent of R_o and by $a_i^R(m,n) = a_i(m,n)R_o$ otherwise. We can then write the function

$$A_i(R_o) = A_i^0 + A_i^R/R_o \tag{4.3}$$

which, together with the set S_R, can be represented as $A_i(R_o^k) = A_i^k, \ \forall k \in \{1,\cdots,\eta\}$. The robustness regarding load variation is achievable by considering all η values of A_i^k during the design. To allow the operation with the extended model, the load must be known and the index $k \in \{1,\cdots,\eta\}$ identified during the converter operation. This determination was done through the estimation of the output resistance.

With the help of this function, we were able to implement the generalization that made the min-type strategies robust to load variations presented in Theorem 1. Table 4.3 presents the control design for the QNS controller, showing the values for $C'C$ and the resulting P matrix for each converter. The optimum objective function is also presented.

Table 4.3: QNS Controllers

Variable	Buck	Boost	Buck-Boost
Design Parameters			
$C'C$	$\begin{bmatrix} R & 0 \\ 0 & 300/R_o \end{bmatrix}$	$\begin{bmatrix} R & 0 \\ 0 & 150/R_o \end{bmatrix}$	$\begin{bmatrix} R & 0 \\ 0 & 30/R_o \end{bmatrix}$
Control Variables			
P	$10^{-3}\begin{bmatrix} 6.4787 & 3.0287 \\ 3.0287 & 9.0551 \end{bmatrix}$	$\begin{bmatrix} 0.2397 & 0.0082 \\ 0.0082 & 0.3453 \end{bmatrix}$	$10^{-2}\begin{bmatrix} 4.8094 & 0.1625 \\ 0.1625 & 6.9038 \end{bmatrix}$
$\mathrm{Tr}(P)$	0.0155	0.5850	0.1171

For the RNS controller, we have solved the conditions of Theorem 2 using the set of equilibrium points S_{ec}^k associated with the set of output voltages $S_r = \{V_e^1, \cdots, V_e^M\}$. For this set, a measurement limitation of 125 V for the output voltage was considered.

As mentioned previously, the values of $C'C$ equal the ones used in the QNS controller. Table 4.4 shows the sets containing the possible points of operation and the matrix product $C'C$ used as input for the control design.

Table 4.4: RNS Controllers

Variable	Buck	Boost	Buck-Boost
Design Parameters			
S_r	$\{5, 10, \cdots, 60\}$	$\{70, 75, \cdots, 120\}$	$\{5, 10, \cdots, 120\}$
$C'C$	$\begin{bmatrix} R & 0 \\ 0 & 300/R_o \end{bmatrix}$	$\begin{bmatrix} R & 0 \\ 0 & 150/R_o \end{bmatrix}$	$\begin{bmatrix} R & 0 \\ 0 & 30/R_o \end{bmatrix}$
Control Variables			
P	$10^{-3}\begin{bmatrix} 6.4787 & 3.0287 \\ 3.0287 & 9.0551 \end{bmatrix}$	$10^{-3}\begin{bmatrix} 3.7451 & 2.8250 \\ 2.8250 & 7.2110 \end{bmatrix}$	$10^{-3}\begin{bmatrix} 1.5289 & 0.8582 \\ 0.8582 & 3.1352 \end{bmatrix}$
$\mathrm{Tr}(P)$	0.0155	0.0110	0.0047

Regarding the sampled min-type strategies, the discrete-time model was determined using a sampling period of $T_s = 25\mu s$, which results in the desired control frequency of 40 kHz.

As we are making online calculation of the system model, the discretization needed to be made during the operation as well. To achieve this without a huge computational cost, we represented the F_i matrix as a function of R_o. To do this, let us take the equation for F_i^k.

$$
\begin{aligned}
F_i^k &= e^{A_i^k T_s} \\
F_i(R_o^k) &= e^{A_i(R_o^k) T_s} \\
F_i(R_o^k) &= e^{(A_i^0 + A_i^R / R_o^k) T_s} \\
F_i(R_o^k) &= e^{A_i^0 T_s} e^{A_i^R T_s / R_o^k}
\end{aligned}
$$

We can then define $F_i^0 = e^{A_i^0 T_s}$ and $F_i^R = A_i^R T_s$, therefore generating the following function.

$$
F_i^k = F_i(R_o^k) = F_i^0 e^{F_i^R / R_o^k} \tag{4.4}
$$

where $e^{F_i^R / R_o^k}$ can be easily calculated during execution. This is because, for the chosen converters, F_i^R only contains one non-zero element and it is on the main diagonal.

Therefore, we have a new set of matrices, from which we can obtain the discrete-time models. The set of functions used in the online discrete-time model is as follows

$$
\begin{cases}
A_i(R_o^k) = A_i^0 + A_i^R / R_o^k \\
F_i(R_o^k) = F_i^0 e^{F_i^R / R_o^k} \\
G_i(R_o^k) = (F_i^k - I)(A_i^k)^{-1} B_i
\end{cases} \tag{4.5}
$$

where $k \in \{1, \cdots, \eta\}$.

With these functions, the implementation of a robust sampled min-type strategy becomes more feasible, allowing us to move on to the control problem. For the RS controllers' design, we have solved the conditions of Theorem 3, choosing beforehand a set S_r and a reliable matrix product $C'C$. These choices aimed to guarantee that the converters operate within their limitations. They can be seen in Table 4.5

With these results, all robust min-type strategies and PWM-based controllers can be implemented. Regarding the control logic, it remains only the steady-state correction methods. An analytical method to design these controllers is yet to be developed. Therefore, the parameters of the PI controller in the correction methods were adjusted empirically during the simulation step.

In Chapter 3, two steady-state correction methods were proposed. A voltage-based method and a current-based method. The first uses the PI to adjust the equilibrium voltage and calculates the equilibrium current based on it. The second uses the PI to adjust only the equilibrium

Table 4.5: RS Controllers

Variable	Buck	Boost	Buck-Boost
Design Parameters			
S_r	$\{5, 10, \cdots, 60\}$	$\{70, 75, \cdots, 120\}$	$\{5, 10, \cdots, 120\}$
$C'C$	$\begin{bmatrix} 0 & 0 \\ 0 & 1 \end{bmatrix}$	$\begin{bmatrix} 0 & 0 \\ 0 & 1 \end{bmatrix}$	$\begin{bmatrix} 0.6 & 0 \\ 0 & 1 \end{bmatrix}$
Control Variables			
P	$\begin{bmatrix} 5.9771 & 3.2050 \\ 3.2050 & 8.6406 \end{bmatrix}$	$\begin{bmatrix} 1.7435 & 1.0341 \\ 1.0341 & 2.8033 \end{bmatrix}$	$\begin{bmatrix} 0.8025 & 0.4054 \\ 0.4054 & 1.2941 \end{bmatrix}$
γ	0.0085	0.0139	0.0034

current while maintaining the equilibrium voltage equal to the reference. Both these converters operate at a sampling period of $T_{ref} = 1$ ms, and the output voltage value used was passed through the filter

$$F(s) = \frac{1.755 \times 10^5}{s^2 + 592.4s + 1.755 \times 10^5} \tag{4.6}$$

which removes the oscillation, leaving out only the steady-state value.

As the objective of these controllers is to correct steady-state errors obtained after applying the min-type switching strategies, the chosen controllers are relatively slow compared to the main loop. As both methodologies for steady-state correction provided a similar performance, we opted to present only the equilibrium current correction method parameters as given in Table 4.6.

Table 4.6: Parameters for the controller used in the current based correction method

Variable	Buck	Boost	Buck-Boost
k_p	0.5	0.5	0.5
k_i	3	3	3

After designing all the controllers, we are ready to compare their performance.

4.2 Comparison of Min-Type and PWM-Based Strategies

This section explores the differences between the proposed min-type switching strategies and the classical PWM-based method. The tests can be divided into two main categories. The first regards increases in the voltage reference through steps. At this first moment, we have not used the steady-state correction method to compare the control methodologies without the influence of an external control loop. The objective is to analyze the transient response, such as stabilization time, current peak, voltage overshoot, and eventual steady-state errors. The second regards output load variations. We can observe the rapid voltage drop, the recovery time during the transient, and the new stabilization voltage.

As shown in the following sections, we have performed the experimental tests with all three topologies from Chapter 2. Hence, giving the readers a broader understanding of the applicability of these switching strategies.

As was already mentioned, we do not consider the external control loop for steady-state correction for most results presented in this chapter. It would alter the control dynamic and hide the natural response of the min-type controllers. Therefore, only specific tests use the correction loop, in which case its use is made explicit.

4.2.1 Buck

In this section, the buck converter was controlled employing the methodologies presented in the previous chapter. The first test consisted of a reference voltage step of 40 V. Figure 4.4 shows the voltage and current responses.

Notice that all min-type controllers had a good step response. Their settling time was very similar, being approximately 22 ms. Also, note that they obeyed the imposed current peak limitation. Comparing with the PI controller, we see a significant improvement. The classical PI approach had a significantly slower response, a little over 40 ms to stabilize. Furthermore, it also suffered from oscillations during the voltage increase. Although these oscillations are not a concerning problem, they are not desirable.

An important aspect that we can also view on these graphs is the similarity between simulation and experiment. Aside from minor differences, the experimental converter behaved as simulated, demonstrating the model precision and giving an idea of its reliability.

Note that the QNS and RNS had an identical response. This similarity is because both present the same Lyapunov matrix $P > 0$. Although strange, this phenomenon is a consequence of this model, where matrices A_i are equal for both subsystems and, therefore, $A_\lambda = A_i \; \forall i \in \mathbb{K}, \lambda \in \Lambda$. Consequently, the restriction imposed during (1) is equal to the one from (2), resulting in practically the same control strategy.

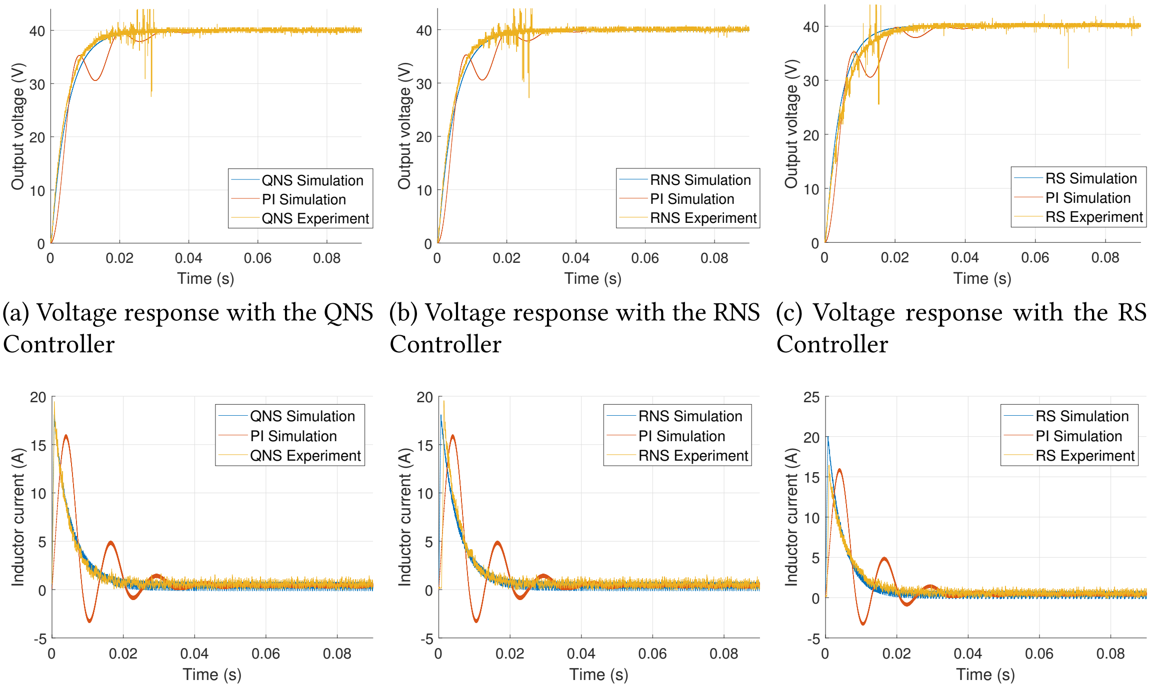

(a) Voltage response with the QNS Controller (b) Voltage response with the RNS Controller (c) Voltage response with the RS Controller

(d) Current response with the QNS Controller (e) Current response with the RNS Controller (f) Current response with the RS Controller

Figure 4.4: Step response of the buck converter operating with min-type controllers.

These results, however, demonstrated the performance for only one output voltage. To verify the design improvement on robustness regarding reference variation, we have to expand this test to other voltage references. It is not practical to show the step response for all equilibrium points considered during the design. Therefore, Figure 4.5 shows only the settling time and current peak values for the converter operation range.

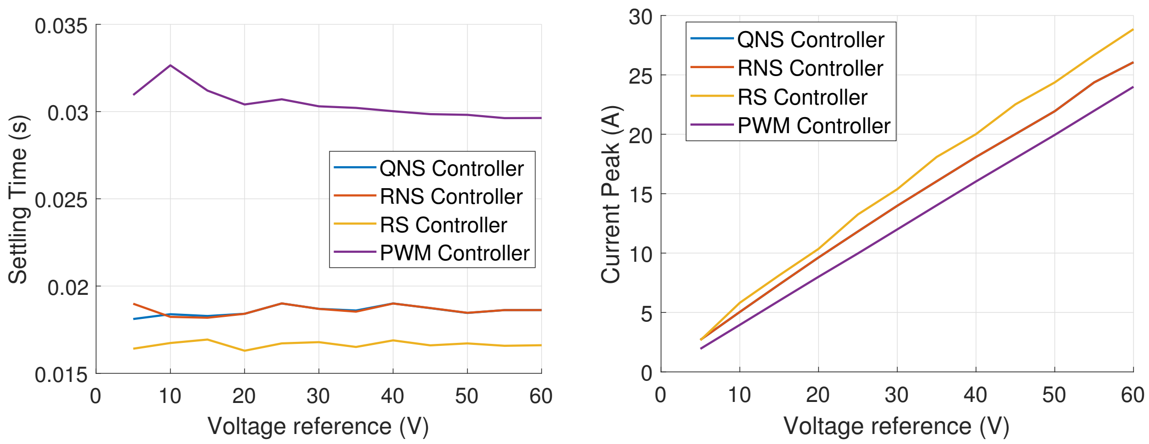

(a) Settling time (b) Current peak

Figure 4.5: Settling time and current peak variations of the buck converter in the range of operation

It is interesting to note that the settling time is kept practically invariant for all the min-type controllers. Although the current peak is not constant, it increases linearly with the output voltage. The only strategy that stands out is the RS, with a slower settling time and smaller current peak. Nevertheless, this discrepancy is due to the design parameters, which are different from those used for continuous-time design. Therefore, it is impossible to perceive a considerable difference between the min-type strategies regarding these performance parameters.

Comparing their results to the PWM-based strategy, we see some apparent differences. The settling time of the PI controller is still relatively stable, but it stays at a much higher value. Despite it being slower than the min-type controllers, the current peak is very similar. In this scenario, the Lyapunov-based controllers had a much better response than the PI, which suffered from the integrator oscillation.

Although Figure 4.5 demonstrates the system robustness regarding reference variations, we have yet to verify the system response to load variations. It is expected for converters to experience changes in the output load; therefore, it is essential to evaluate the converter's performance in this scenario. Furthermore, through these tests, we can assess the effectiveness of the design generalizations proposed in Chapter 3.

Without specialized equipment, it is impractical to evaluate the converter behavior at a wide range of load resistances. Therefore Figure 4.6 contains only simulation data. It presents the observed steady-state error of the min-type strategies with loads varying from $0.1R_o$ up to $2R_o$, at steps of $0.1R_o$. For the sake of comparison, this figure presents the result of the control methodology proposed in [30] which is the same control technique proposed in Chapter 3 but without the generalization to cope with load variations.

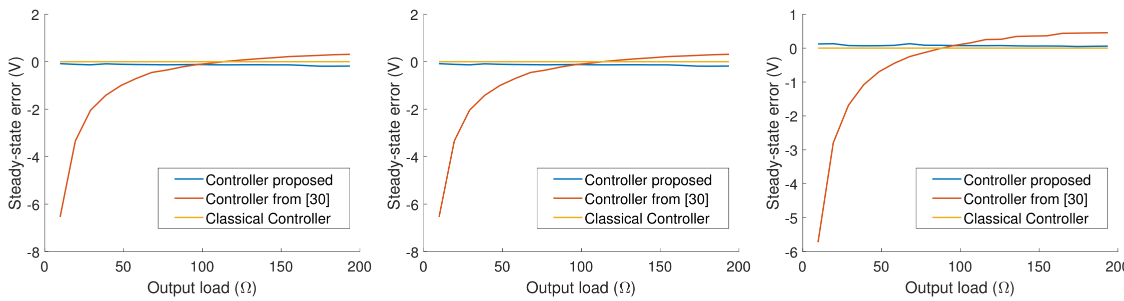

(a) QNS Controller (b) RNS Controller (c) RS Controller

Figure 4.6: Steady-state error of the buck converter using the min-type controllers for each output load.

The graphs from Figure 4.6 are very similar for all min-type controllers and present some interesting results. The voltage error reached more than 6 V for small resistance values for the technique proposed in [30], representing an error of more than 15%. This error is less perceivable for higher resistance values. However, it is significant whenever the value is smaller than the R_o used for the design. These results reduce the applicability of the min-type switching strategies proposed in [30]. However, when the load variations are taken into account during the control design, enabling the load estimation during the converter operation, the error is practically non-existent. Its steady-state error curve is very similar to that of the PI controller, which has a null error due to its integrative component.

Although very good, these results are only simulations and do not show the transient response. Therefore, we also made an experimental load step test. A rapid resistance decrease happens by adding a parallel load, which takes it from 96.8Ω to 48.4Ω. Figure 4.7 shows the voltage behavior during this variation and compares the experimental results to the simulation and the PWM-based PI controller. As the voltage drop tends to be relatively small, any voltage error is perceivable. Therefore, to facilitate the comparison, a steady-state correction strategy from Chapter 3 is used with the min-type controllers, specifically the current method.

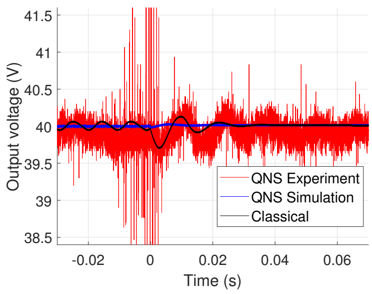

(a) QNS Controller

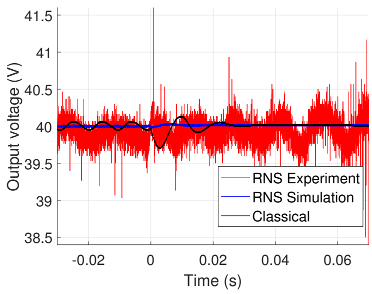

(b) RNS Controller

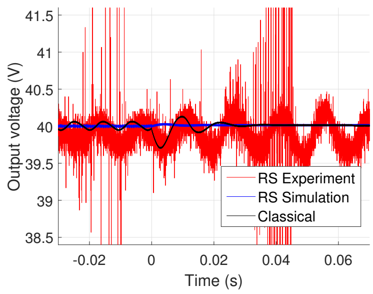

(c) RS Controller

Figure 4.7: Voltage response to a 50% output resistance drop on the the buck converter.

The graphs from Figure 4.7 present another great result from the load estimation. The voltage variation is almost non-existent, being even smaller than the ripple magnitude. When compared to the PWM-based strategy, the improvement is even more visible. The PI relies on the voltage drop to correct the PWM duty-cycle, so a voltage decrease is inevitable. However, min-type controllers operate differently. They use the output current to estimate the load and alter the control rule. Therefore, it is capable of instantaneous control adjustments.

4.2.2 Boost

Figure 4.8 presents the step response for the min-type control strategies and compares them to the classical approach with the PI controller. We have adopted a reference voltage step of 110 V and no correction method at this first moment.

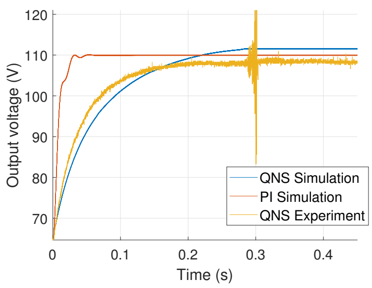

(a) Voltage response with the QNS Controller

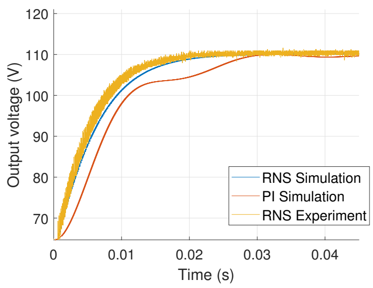

(b) Voltage response with the RNS Controller

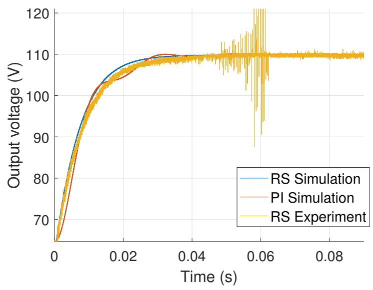

(c) Voltage response with the RS Controller

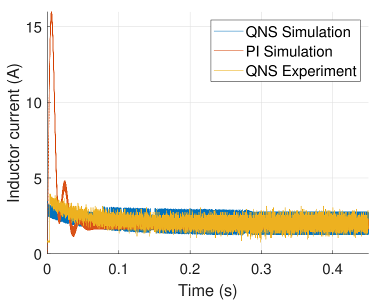

(d) Current response with the QNS Controller

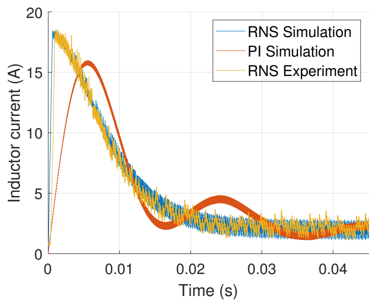

(e) Current response with the RNS Controller

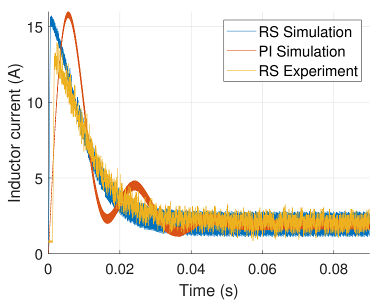

(f) Current response with the RS Controller

Figure 4.8: Step response of the boost converter operating with min-type controllers.

Differently from what happens with the buck converter, the min-type strategies step responses are no longer equal in Figure 4.8. The QNS controller is the most divergent of them. The settling time is significantly higher, approximately 230 ms, which is slow compared with the RNS, RS, and PI controllers. They have settling times of 28 ms, 40 ms, and 60 ms, respectively. Another visible disadvantage of the QNS controller is the steady-state error, which is approximately 2 V. This is not very high when considering the 110 V adopted as reference. However, it is multiple times higher than the error from other min-type controllers.

All these aspects are clear disadvantages of the QNS control strategy. However, its slower response allows the controller to perform voltage steps with almost no current peak. The current values perceived during the transient are similar to the ones from the steady-state operation. This aspect in the control response enables a rapid rise of the converter voltage to even higher values without requiring a voltage ramp.

Regarding the RNS and RS control responses, we perceived intriguing results. The system stabilizes rapidly and with no voltage oscillations, which does not happen with the designed PI. The current peak is much higher now than with the QNS controller. However, the steady-state error is now practically non-existent. These results strengthen the idea that these min-type control strategies present some advantages compared to the classical approach.

We conducted more tests through simulations to supply a more vast understanding of the performance of these control strategies at a broader range of output voltages. Figure 4.9 shows the settling time and current peak of the converter step response for each equilibrium voltage considered during the design.

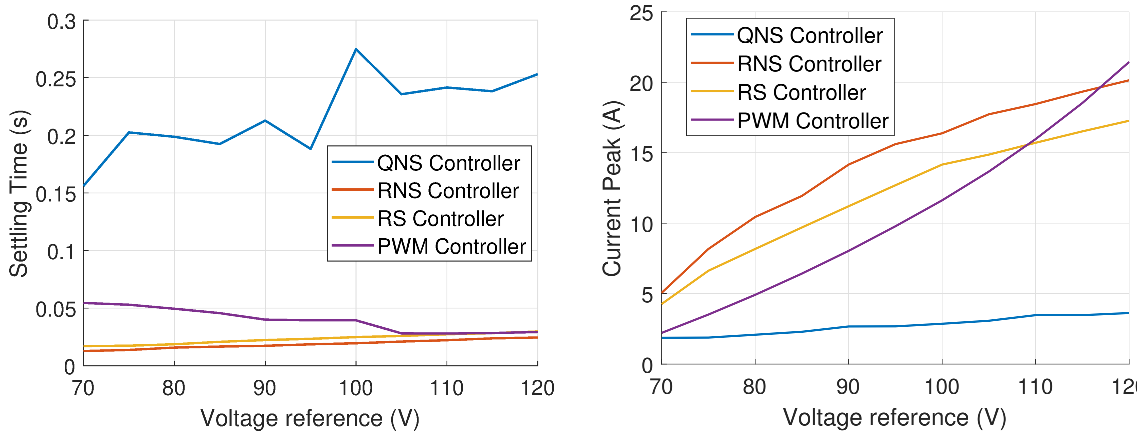

(a) Settling time

(b) Current peak

Figure 4.9: Settling time and current peak variations of the boost converter in the range of operation

The current peak graph for the QNS controller is almost constant, suffering slight variation with the output voltage increase. This small variation strengthens the idea that this control strategy might pose an option to remove the need to perform a ramp increase of the voltage during startup. The current for the other controllers has a more regular pattern compared to the buck converter tests. However, the peak current of the min-type strategies tends to increase slower at higher voltages for the tested values. Meanwhile, the opposite happens with the PWM-based approach. It is important to remember that the approximated system model adopted in the classical controller (2.26) considers a reference voltage of V_e = 110 V and, therefore, it is expected to obtain a better performance near this value.

Figure 4.9 shows the system robustness regarding different output voltages; however, another widespread scenario that also requires robustness is when the resistance of the output load varies. Due to this scenario, we proposed the control design generalizations for the min-type controllers in Chapter 3. We have not yet seen these improvements on the boost converter in the literature to date. To make such an evaluation, we have used the same tests presented in the buck section.

Through simulations, the output resistance varied from $0.1R_o$ up to $2R_o$ at steps of $0.1R_o$. Forcing the converter to operate with all resistances considered during the design. The voltage error observed with each controller is presented in Figure 4.10. For each min-type control strategy, we presented the result with and without the control improvements.

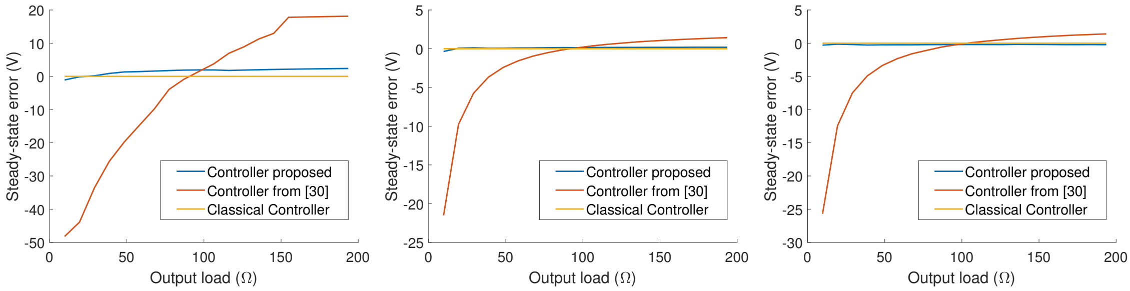

(a) QNS Controller (b) RNS Controller (c) RS Controller

Figure 4.10: Steady-state error of the boost converter using the min-type controllers for each output load.

Note that for all min-type controllers, the load estimation, together with the control design changes, results in a significant enhancement of the adopted control technique. Regarding the RNS and the RS control strategies, the steady-state error becomes almost zero in all operation range. This small value represents a significant improvement compared to the technique proposed in [30], especially for lower resistances. Regarding the QNS controller, without the control alteration, the voltage error was very high, reaching values up to 40%. The design improvement reduced this error to a maximum of 5%, which is still relatively far from the null error obtained by the PI; nonetheless, it is a significant control improvement.

To better understand the transient response during one of these load changes, we conducted an experimental load step test. The output resistance was abruptly halved through the use of a controlled parallel load, resulting in a resistance decrease from 96.8Ω V to 48.8Ω.

As it was noted in (4.10), the min-type strategies are prone to steady-state error, albeit it is usually small. However, as it will be seen, the load step test results in voltage variations even smaller. Therefore, to help the visualization, a steady-state correction technique was used, specifically the current correction. Figure 4.11 shows the results of this test.

The simulation and experiment of the load step test provide a meaningful conclusion. The min-type strategies working with the load estimator can quickly adjust to load changes without

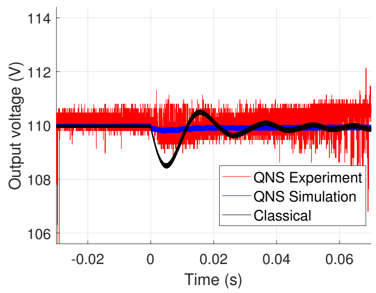

(a) QNS Controller

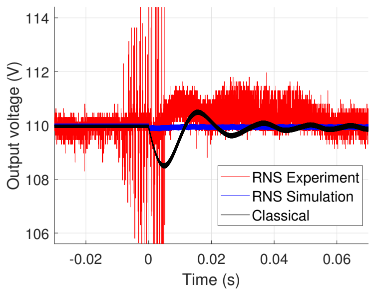

(b) RNS Controller

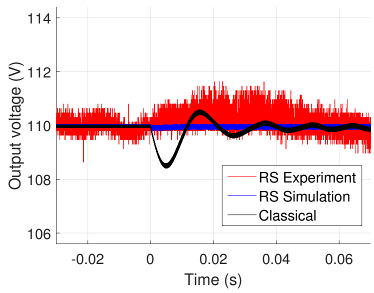

(c) RS Controller

Figure 4.11: Voltage response to a 50% output resistance drop on the the boost converter.

the need for a voltage drop, as occurs with the PWM-based PI controller. The variations are almost not perceivable, having a smaller magnitude than the steady-state ripple. The classical method has a very different behavior, with a much higher voltage drop and recovery time.

4.2.3 Buck-Boost

Figure 4.12 presents the step responses for the min-type control strategies and compares them to the classical approach with the PI controller. We have adopted a reference voltage step of 100 V and no correction method at this first moment.

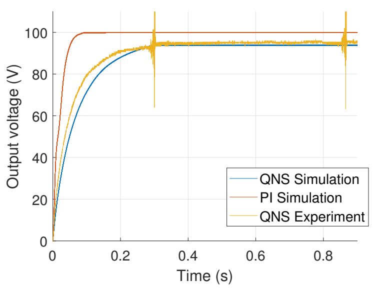

(a) Voltage response with the QNS Controller

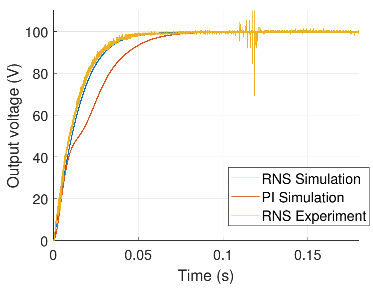

(b) Voltage response with the RNS Controller

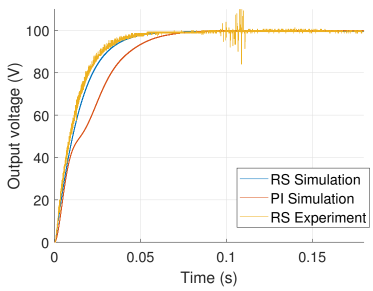

(c) Voltage response with the RS Controller

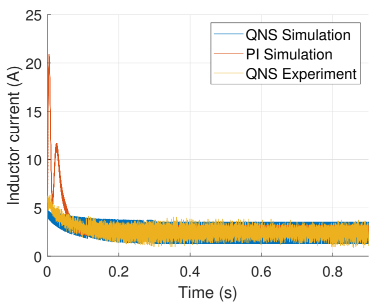

(d) Current response with the QNS Controller

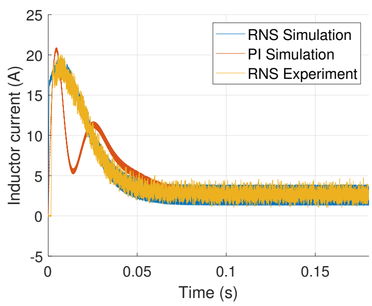

(e) Current response with the RNS Controller

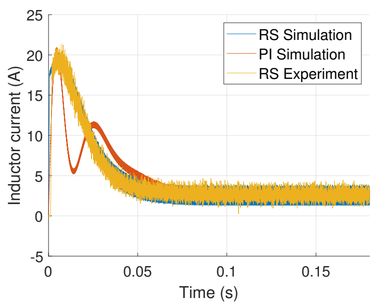

(f) Current response with the RS Controller

Figure 4.12: Step response of the buck-boost converter operating with min-type controllers.

Regarding the QNS controller response, some aspects stand out. Concerning the voltage response, the stabilization is significantly slower than any other controllers, happening only at 270 ms. Moreover, the converter also suffers from a steady-state error of approximately 6%, which is too high to be ignored. However, for the current response, it did not experience a significant peak during startup, attaining values relatively close to the ones from the steady-state operation.

Albeit the poor behavior of the QNS controller, the RNS and RS controllers presented a much different result. Both have a relatively similar response and outperform the PI controller. The peak current is approximately 20 A. The voltage stabilizes with no practical steady-state error at 60 ms for both RNS and RS controllers.

Extending the step analysis to other voltage references, Figure 4.13a presents the settling time for all voltage values considered during the control design.

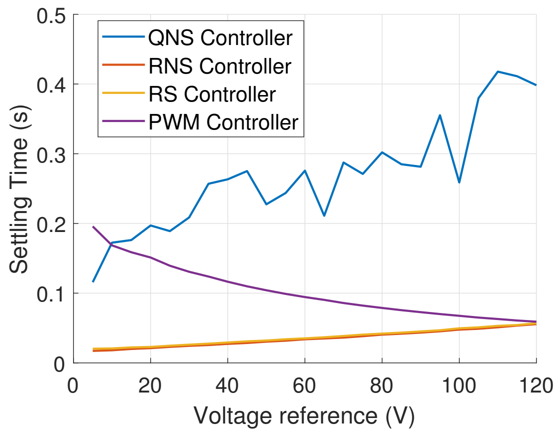

(a) Settling time

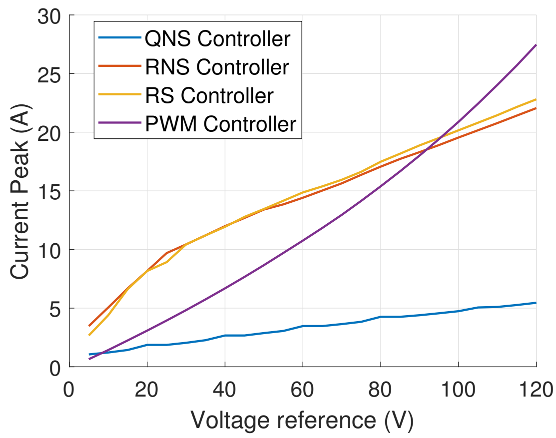

(b) Current peak

Figure 4.13: Settling time and current peak variations of the buck-boost converter in the range of operation

As it was already observed in Figure 4.12, Figure 4.13a also demonstrates that the behavior of both the RNS and RS controllers are considerably similar. Both outperform the PWM-based controller within the range of operation. The QNS, however, is outperformed by the PI for most voltages. It is only slightly faster at slower references. However, this is due to the PI design consideration of the linearized model, which we obtained for a very different operation point.

Regarding the settling time variation, some aspects are interesting to note. Firstly, the settling time for min-type strategies tends to increase at higher voltages; however, the opposite occurs with the PI. Also, the settling time variation on the RNS and RS controllers is small compared to the PI. This proximity indicates that these min-type strategies are well adjusted to reference changes.

In the current peak variation from Figure 4.13b, it is visible that the PWM-based controller tends to have a smaller peak at lower voltages. However, it increases rapidly with the voltage increase, eventually surpassing all min-type strategies. Notice, however, that this higher peak does not result in a shorter settling time.

These results demonstrate the robustness of the RNS and RS controllers regarding reference variations, even outperforming the PI used with the PWM. However, we have yet to evaluate the performance of these strategies for load variations with the buck-boost converter. With this objective, through simulations, a new test was made using these same controllers. At a constant voltage reference, the output load varied from $0.1R_o$ to $2R_o$ with steps of $0.1R_o$. For the sake of comparison, we also verified the behavior of the min-type controllers with the methodology proposed in [30], which disregards load variation during the control design step. Figure 4.14 shows the steady-state error observed during this variation.

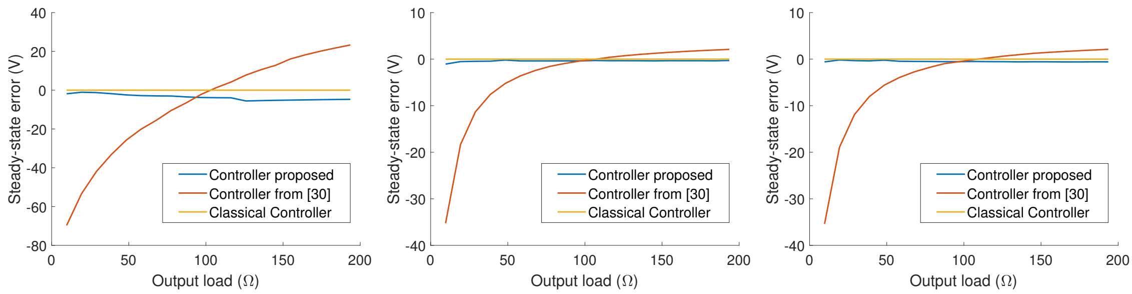

(a) QNS Controller (b) RNS Controller (c) RS Controller

Figure 4.14: Steady-state error of the buck-boost converter using the min-type controllers for each output load.

As is expected, the PI's integrator enables it to maintain a zero-error operation regardless of the output load. However, the most remarkable result from Figure 4.14 is the steady-error reduction, which is possible due to the load estimation and the online model change.

However, albeit the improvement, the QNS controller still experiences significant voltage errors, even with the load estimator. However, both the RNS and RS controllers manage to operate with minimal error. The maximum observed mean voltage difference is 1 V.

To demonstrate transient behavior during a load change, Figure 4.15 shows the voltage response for an output resistance reduction. As the voltage drop during the test is considerably small, we enabled the steady-state current correction method proposed in Chapter 3. This correction makes sure that all controllers are operating at precisely the same voltage.

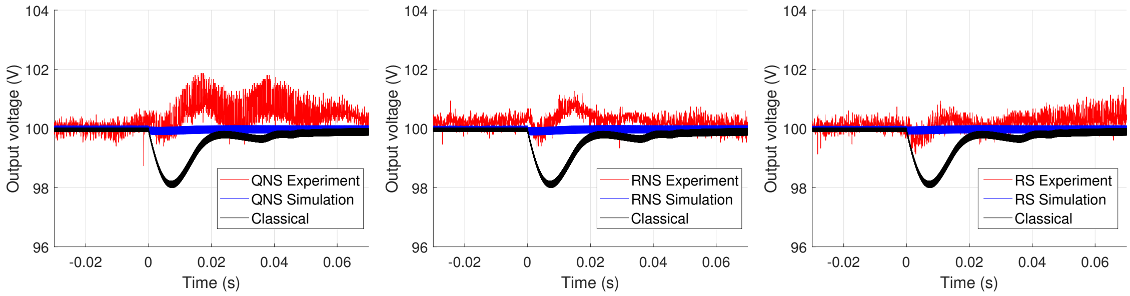

(a) QNS Controller (b) RNS Controller (c) RS Controller

Figure 4.15: Voltage response to a 50% output resistance drop on the the buck-boost converter.

Figure 4.15 contains the most significant result from the use of the load estimator. The min-type strategies almost do not experience a voltage drop during the load change. When compared to the classical controller, the result is even more interesting. The PI controller relies on the voltage drop to adjust the PWM duty-cycle; therefore, it cannot operate with a minimal voltage drop. The min-type controllers use the output current to estimate the load. Therefore, they can instantly notice the load change, which allows the converter to have a faster response.

4.3 Chapter Considerations

We experimentally tested the buck, boost, and buck-boost converters with min-type strategies and their response compared to a PWM-based controller throughout this chapter. The objective was the evaluation of the advantages and disadvantages of the proposed control strategies. We made tests to evaluate the enhancement obtained in the results thanks to the control design generalizations concerning robustness regarding changes in the equilibrium point and load variations.

The results obtained through simulations and experimental tests provided readers with a diverse understanding of the min-type control strategies. The graver observed problems are the settling time and steady-state error of the QNS controller when operating the boost and buck-boost converters. However, the remainder control strategies had an excellent response during the reference steps and load variations. With them, the settling-time was always smaller or similar to the PWM-based controller.

Regarding the load robustness, we presented some interesting effects of the design change proposed. The load estimation significantly reduced the steady-state error, which could reach very high values depending on the load. Furthermore, almost no voltage drop occurs during a load step, which is a significant result, even compared to the PWM-based controller.

When considering the external control loop responsible for the steady-state correction, a non-zero operation is possible, solving one of the gravest problems. To further minimize the disadvantages of the min-type strategies, future works have an opportunity to improve the control design, removing the need for an online update of the output resistance. However, the results presented here indicated many advantages of the min-type controllers. They support the thought that these control strategies should be considered a real alternative to standard control techniques.

Chapter 5

Switching Frequency Analysis

This chapter is dedicated to studying the switching frequency behavior of min-type switching strategies. As it will be clear throughout this chapter, while the PWM-based strategy always operates in the maximum switching frequency, these strategies present an intrinsic property characterized by a variable switching frequency that depends on the operation point. Generally, this frequency is smaller than the control frequency, indicating a great potential for power loss reduction compared to conventional techniques. In this chapter, experimental and simulation tests were made to obtain the frequency profile for each converter to verify the switching frequency variation according to the output voltages.

5.1 A Brief Literature Review

The switching frequency of min-type control strategies has already been the subject of some studies, such as [26, 28]. The interest in the switching frequency of these controllers comes from a place of concern. The non-sampled control strategies presented in [10] were used as a base for many studies, such as [18]. However, they suffer from a known problem regarding the switching frequency. These controllers can assure asymptotic stability because they assume an infinity switching frequency around the equilibrium point, which is not valid for real applications.

As demonstrated in this chapter, when the control frequency is sufficiently high, the converter response becomes very similar to asymptotic stability. However, as the control frequency decreases, the difference between the theoretical and practical results becomes evident, both through ripple and steady-state error.

Many studies tried to improve these control strategies and solve this frequency limitation, usually by imposing Dwell-Time restrictions on the switching rule. To reduce the theoretical and practical gaps, reference [3] has proposed a technique to reduce the switching during the transient while [26] has presented a control technique based on a continuous-time model with Dwell-Time guarantees. Reference [9] also presented a control strategy with dwell-time guarantees, but based on a specific discrete-time model equivalent to the associated sampled-data continuous-time system.

These studies focused on control frequency limitation. They even developed the sampled min-type controller, which has been used as a basis for the RS controller presented throughout this dissertation. All these references were essential to reduce the gap between theory and practice. However, we have not yet seen a study that approached this frequency variation as a means of possible power reduction capabilities. Studies (see [1, 16, 20]) have shown that, unless the converter operates at very low power, switching losses represent a significant portion of the power lost in power converters. PWM-based control strategies operate at a constant switching frequency unless a frequency variation algorithm is implemented (see [22]). As it will be further seen here, the min-type strategies do not operate at a constant switching frequency. Therefore it might be capable of reducing power losses without the need for any additional algorithm. To verify this hypothesis, in [30] we showed how the switching frequency varies in the buck-boost converter operating with min-type strategies.

This chapter explores the frequency variation of min-type controllers of the buck, boost, and buck-boost converters. The objective is to verify if these control strategies present a switching frequency profile, which allows a power loss reduction compared to a constant frequency switching.

To avoid confusion, let us remember some definitions already presented in the previous chapter. Control frequency refers to the execution rate of the control routine. Commutation frequency refers to the number of commutations of the switching rule per second. Meanwhile, switching frequency denotes the frequency of the PWM signal. As during a period of the PWM signal occurs two subsequent commutations, the maximum commutation frequency is always double the switching frequency.

5.2 Buck

Before evaluating the real commutation frequency, let us verify its behavior through simulations. As a first test, we have verified the influence of the control frequency on the switching. With this purpose, we have evaluated through simulations the commutation frequency at three different common control frequencies (1 MHz, 200 kHz, and 40 kHz). This result can be observed in Figure 5.1. Note that the experimental converter gates and gate drivers would have to change to operate the converter at these frequencies. Therefore we did not consider the gate driver dead-time during these simulations.

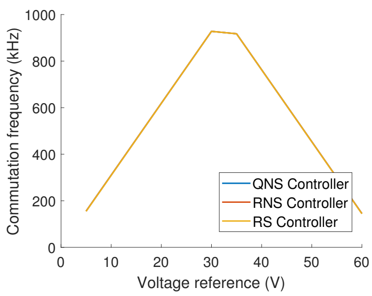

(a) Switching frequency with a 1 MHz controller

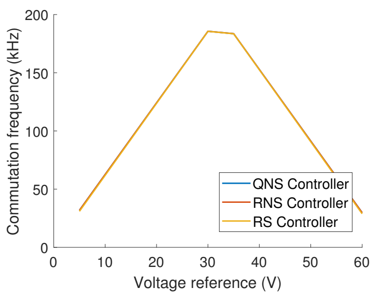

(b) Switching frequency with a 200 kHz controller

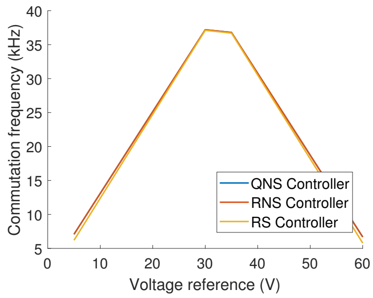

(c) Switching frequency with a 40 kHz controller

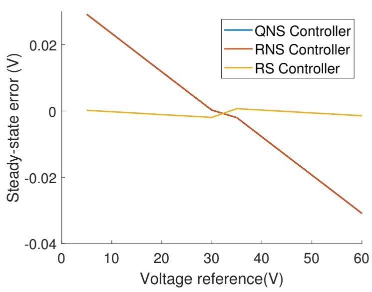

(d) Voltage error with a 1 MHz controller

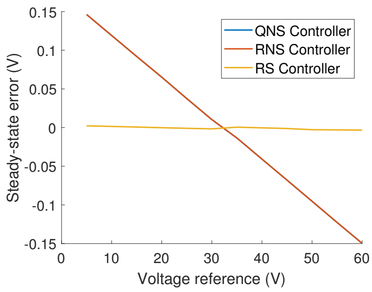

(e) Voltage error with a 200 kHz controller

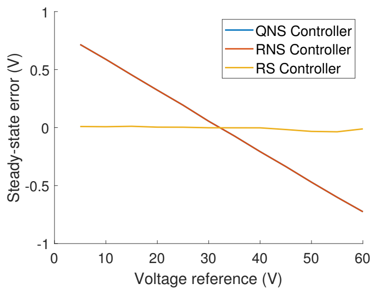

(f) Voltage error with a 40 kHz controller

Figure 5.1: Buck converter using the min-type controllers at different control frequencies.

Some interesting behaviors are noticeable. The frequency pattern is very similar for all control frequencies. It has a well-defined peak at half the input voltage, with a significant frequency reduction at low or high voltages, reaching values approximately 8 times smaller at both extremes. As switching losses are proportional to the frequency, this might potentially cause a very significant efficiency increase for applications that must operate with a variable voltage reference.

Another result presented in Figure 5.1 is the steady-state voltage error perceived at each of these converters. Note that both RNS and QNS controllers have identical behaviors. Compared to the RS controller, they tend to have a higher error. In contrast, the RS controller has almost no voltage deviation for all the tested range of operation. The error pattern is also very similar at all the tested control frequencies. However, note one important difference. The control frequency decrease causes the increase of the steady-state error. The design of each controller can explain this phenomenon. The non-sampled controllers consider the continuous-time model and assure asymptotic stability. However, this model does not consider any constraint in the switching frequency. Consequently, they require an infinity switching frequency to attain equilibrium. As a switching limit is imposed and decreased, the system differs from the theoretical model considered for the design. This model difference then results in a voltage deviation.

In contrast, the sampled controller is not affected by this model divergence. It considers the discrete-time model, which already imposes a frequency for the control. The minor voltage error observed, in this case, is caused by the fact that the sampled controller only assures practical stability around the equilibrium point. Therefore some voltage error might occur, although it is usually small.

Note that the results from (5.1) were obtained through simulations still with a relatively ideal system. We can replicate the test with the real converter. As explained during Chapter 4, the experimental tests were made at a control frequency of 40 kHz, which results in a maximum switching frequency of 20 kHz, which is within the frequency limitation of the gate. Hence, we can enhance the simulation by considering the dead-time. The simulation and experimental results can be seen in Figure 5.2. In this test, to guarantee that the reference voltage corresponds to the reality, the current steady-state correction method was used.

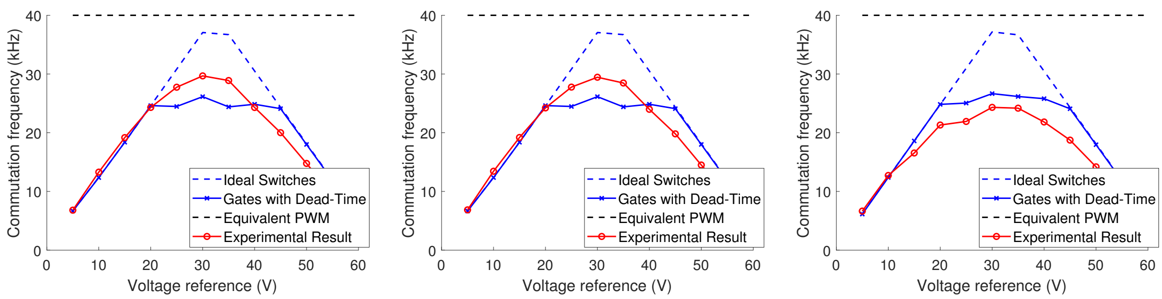

(a) QNS Controller (b) RNS Controller (c) RS Controller

Figure 5.2: Switching frequency of the buck converter for each reference voltage using the min-type controllers.

As it could be expected, all controllers had a very similar result. The dead-time has a significant impact on the frequency pattern, practically imposing an upper limit for the commutation frequency. Due to this limitation, the frequency reduction magnitude at low and high voltages is no longer high. However, it is still relevant and possibly capable of a significant power loss reduction. Another relevant aspect in these graphs is the similarity between experimental and simulation. Although there are some differences, the pattern similarity is easily visible. If a more accurate model were used for the simulations, considering sensor noises, capacitor resistance, and other control delays, the result would probably be even more similar.

5.3 Boost

Now using the boost topology, we replicated the tests performed on the buck converter. We verified the commutation frequency pattern at multiple control frequencies and its influence on the steady-state error through simulations. The tests considered the control frequencies of 40 kHz, 200 kHz, and 1 MHz to cover a wide range of operations. The results can be seen in Figure 5.3. Once again, for these results, the dead-time of the gate driver was not considered.

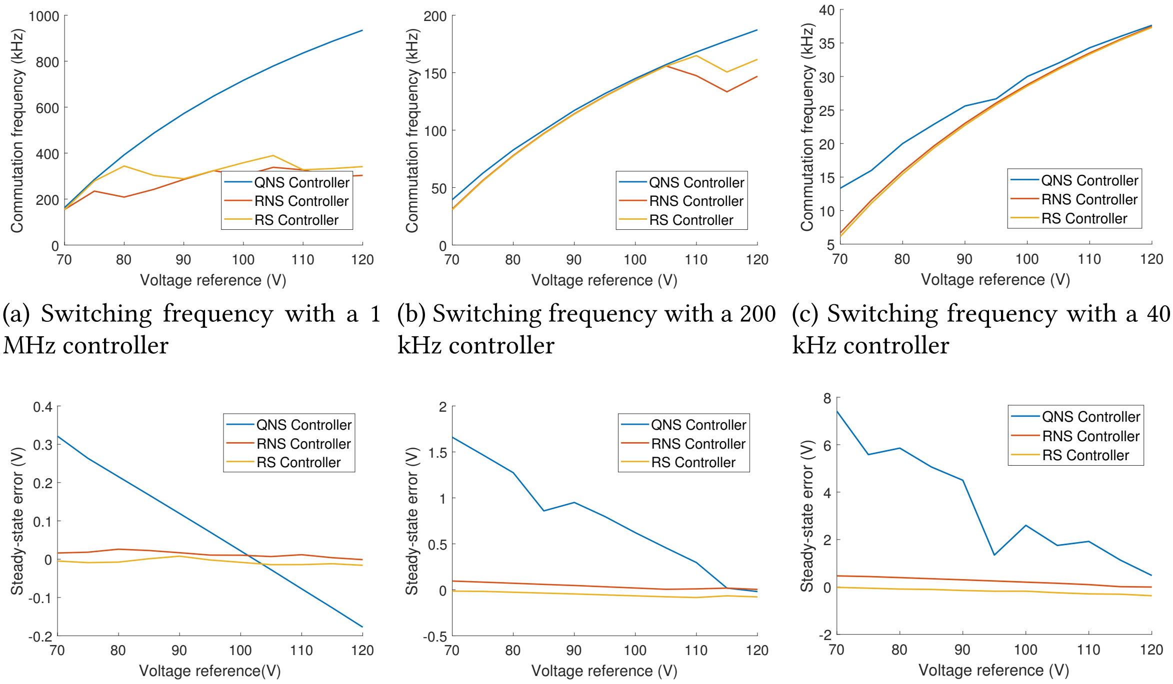

(a) Switching frequency with a 1 MHz controller
(b) Switching frequency with a 200 kHz controller
(c) Switching frequency with a 40 kHz controller
(d) Voltage error with a 1 MHz controller
(e) Voltage error with a 200 kHz controller
(f) Voltage error with a 40 kHz controller

Figure 5.3: Boost converter using the min-type controllers at different control frequencies.

Albeit being the same test, the results here differ significantly from the buck converter. There is a noticeable pattern change with the RNS and RS controllers, depending on the control frequency. At 1 MHz, these controllers have a relatively small frequency variation, which would probably not culminate into an exciting efficiency improvement. However, with the control frequency decrease, at 200 kHz and 40 kHz, the pattern becomes more promising, becoming almost linear with the voltage increase. Therefore, at low power, where switching losses are relevant, the switching is less frequent, resulting in power loss reduction, consequently, in an efficiency improvement.

Regarding the steady-state error, Figure 5.3 reveals that similar to what happened with the buck converter, the reduction in the control frequency causes the increase of the voltage error. Again, with the RNS and RS controllers, the error is relatively small. However, when operating with the QNS min-type strategy at 40 kHz, the error reaches almost 8 V for a 70 V reference, which is very high. Therefore, the external correction loop might be essential for its proper operation.

Figure 5.3 presented a frequency pattern with a great potential for efficiency improvement. However, we have yet to verify if the same behavior is observable within the actual converter. We conducted the same test with the experimental converter at a control frequency of 40 kHz with this objective. Besides the experimental test, we can also improve the simulations by considering the dead-time of the gate driver. These results are presented in Figure 5.4. This new test used the steady-state correction method to avoid the voltage error observed during the previous simulations.

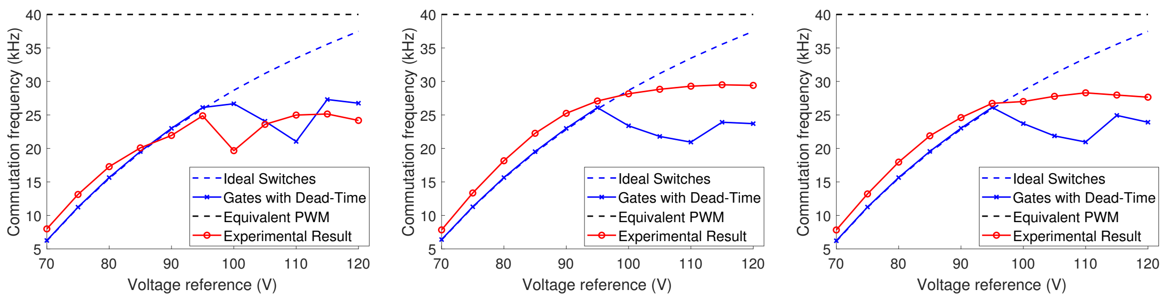

(a) QNS Controller (b) RNS Controller (c) RS Controller

Figure 5.4: Switching frequency of the buck converter for each reference voltage using the min-type controllers.

Note that the frequency pattern of the QNS controller with ideal switches is visibly different from what was observed previously in Figure 5.3. Now QNS behaves in a much similar way to the other min-type strategies. This change is due to the correction method forcing the converter to operate at a different equilibrium point, matching the voltage reference.

Similar to the buck, the dead-time consideration influenced the commutation frequency. The controller ceases to reach higher frequencies, stagnating at a maximum of approximately 25 kHz. This behavior is relatively similar in the experimental converter, except for some minor variations. The frequency stagnation observed with the real converter and the more accurate simulation might raise some concerns. However, an unmistakable resemblance between this pattern and algorithms that change the PWM frequency to improve efficiency is visible [1, 16]. This similarity indicates the potential of the min-type switching strategies.

5.4 Buck-Boost

Finally, let us verify the frequency variation pattern on the buck-boost topology. Once again, we verified the commutation frequency pattern at three different control frequencies (1 MHz, 200 kHz, and 40 kHz). As the experimental converter specifications are not compatible with all these frequencies, the tests consisted of only simulations. The switches were considered ideal, without any delay. The result of these simulations can be observed in Figure 5.5.

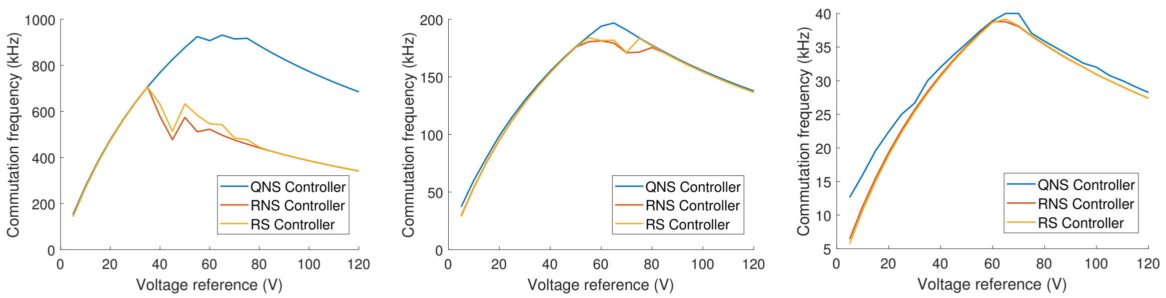

(a) Switching frequency with a 1 MHz controller (b) Switching frequency with a 200 kHz controller (c) Switching frequency with a 40 kHz controller

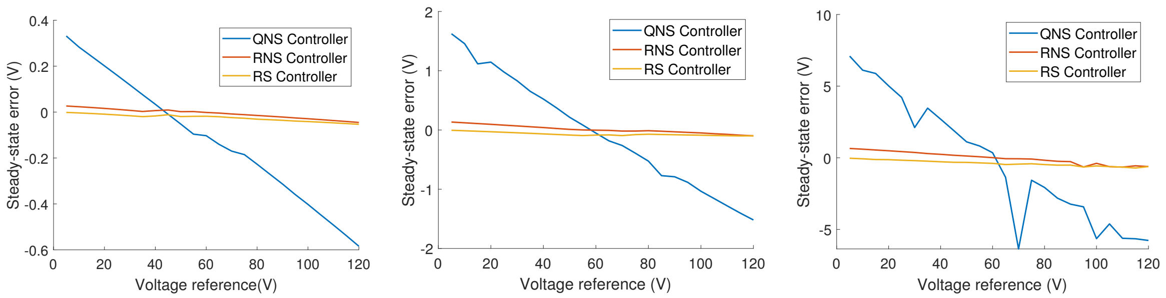

(d) Voltage error with a 1 MHz controller (e) Voltage error with a 200 kHz controller (f) Voltage error with a 40 kHz controller

Figure 5.5: Buck-Boost converter using the min-type controllers at different control frequencies.

Like the boost, the frequency pattern in the min-type switching strategies converges to the same curve as the control frequency decreases. At 1 MHz, the QNS behavior differs significantly from the RNS and RS controllers, which have a much smaller frequency peak, which also happens at a lower voltage. As the control frequency decreases, the pattern tends to a more triangular form. The peak occurs when the output voltage is close to that of the input, that is 65 V.

Regarding the steady-state error, it can be noticed that it is practically inversely proportional to the frequency. Although in the RNS and RS controllers, the perceived error was relatively small during all simulations. However, the same is not valid for the QNS controller. Even at a control frequency of 200 kHz, the error already reaches values greater than 1.5 V, which is very high for low voltages. This problem is very significant at 40 kHz. In this case, the error can reach values greater than 7 V. This shows the importance of an external correction loop for the proper operation of the control strategy.

After the discoveries from the simulations, we focused on verifying the real converter behavior. For this, we focus on the 40 kHz control frequency to guarantee that the maximum switching frequency does not surpass the gates limit. To guarantee that the output voltage matches the reference, we used the steady-state correction method. Figure 5.6 shows the test results. As a base of comparison, we also provided simulation results, demonstrating the frequency pattern with the dead-time and with ideal switches.

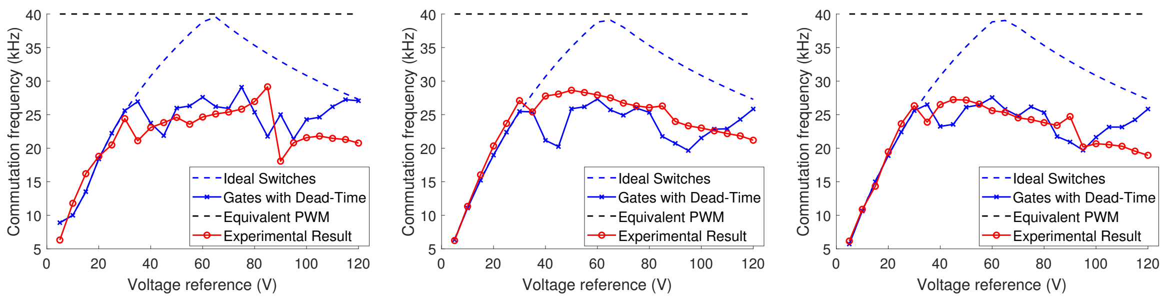

(a) QNS Controller (b) RNS Controller (c) RS Controller

Figure 5.6: Switching frequency of the buck converter for each reference voltage using the min-type controllers.

As it happened with the other converters, the frequency pattern of all the control strategies was very similar. The deformations on the curve of the QNS controller, which could be seen in Figure 5.5, are not present in the ideal switches curve from Figure 5.6. This difference is due to the steady-state correction method, which guaranteed that the output voltage matched the reference.

Note that the considerations of the dead-time in the simulations caused a significant change in the pattern. As it happened with the other converters, the frequency stagnates at a particular value, presenting minimal variation. This frequency limitation impacts the power loss reduction capabilities; however, the frequency variation is still very significant at lower voltages. Hence, it could still result in a reasonable efficiency improvement.

5.5 Chapter Considerations

We evaluated the behavior of the buck, boost, and buck-boost converters regarding the control frequency and the commutation frequency throughout this chapter. Our objective was to verify if the min-type switching strategies might improve the converter's efficiency due to its inherent switching frequency variation.

The results obtained through the simulations provide some very relevant insights. Firstly, the steady-state error is inversely proportional to the control frequency of the min-type controllers. Also, as this frequency decreases, the switching of all control strategies tends to the same curve. When considering the experimental results, we observed stagnation of switching frequency due to the gate drivers' dead-time. Although the curve flattening impacts the magnitude of the frequency variation, there is still a voltage range in which a significant frequency variation occurs with all the converters. This variation might reduce the switching losses and increase the converter efficiency within the range.

We have, therefore, achieved our goal of verifying the frequency pattern. As already mentioned, the profile might result in a relevant power loss reduction. Future works may deepen the analysis through the actual verification of the power losses and compare it to PWM-based controllers.

Chapter 6

Conclusion

The main goal of this dissertation was to explore the application of min-type control strategies in DC-DC power converters. We verified if these controllers are valid options for real applications. Accordingly, we evaluated the advantages and disadvantages of this control scheme and compared it to the classical PWM-based approach.

We tested three min-type switching strategies throughout the study. Each of these had unique characteristics. The Quadratic Non-Sampled (QNS) design considers operation within the whole equilibrium region. The Robust Non-Sampled (RNS) is less conservative, and its design considers specific equilibrium points. The Robust Sampled (RS) uses a discrete-time model and considers frequency limitations during the design. These control strategies are all derivations of previous studies (see [9, 10]). Albeit the similarity, we proposed some relevant design improvements. Our generalizations make the system robust to load changes and to reference variations [30]. Besides the design enhancement, we proposed an external control loop to avoid any steady-state error. We explored two different correction methods and applied one of them throughout the study.

We designed these control strategies to operate some DC-DC converters. We delved into three different topologies: buck, boost, and buck-boost. The circuit variation enabled us to analyze the response of the control strategies in multiple scenarios, giving readers a broader knowledge of their applicability. To serve as a base of comparison, we also discussed the classical PWM-based approach. We explored a technique for the design of the PI showing its control scheme. We then made the desired analyses with the experimental converter.

The results from Chapter 4 demonstrated the impact of the control design improvements from Chapter 3. All rules are now robust to changes in the equilibrium point and manage to operate the converters with good performance and reliability. Regarding load variations, the results were even more remarkable. The min-type strategies are now robust to load variations. The load estimator also enables the system to adapt to any change quickly. Even during an abrupt load variation, the estimator instantly adapts the switching rule. These results support the idea that min-type control strategies pose a real alternative to the classical approach.

Furthermore, aside from the transient and steady-state voltage responses, we also explored the switching frequency of these controllers. Due to the nature of the min-type switching rules, the switching frequency varies with the point of operation. Many efficiency improvement methods rely on frequency variation to reduce switching losses on PWM-based controllers. Some of these novel frequency profiles resemble those enforced by these methods, supporting the thought that they may increase the converter efficiency.

In summary, we achieved our primary goal of demonstrating the applicability of min-type converters and raise their advantages and disadvantages. Further studies might focus on developing a control rule capable of adapting to load changes without real-time adaptations on the model. This improvement would reduce the processing time and enable operation at higher frequencies.

Bibliography

[1] J. A. Abu Qahouq, O. Abdel-Rahman, L. Huang, and I. Batarseh. “On Load Adaptive Control of Voltage Regulators for Power Managed Loads: Control Schemes to Improve Converter Efficiency and Performance”. In: *IEEE Transactions on Power Electronics* 22.5 (2007), pp. 1806–1819. DOI: 10.1109/TPEL.2007.904232.

[2] M. Agostinelli, R. Priewasser, S. Marsili, and M. Huemer. “Fixed-frequency Pseudo Sliding Mode control for a Buck-Boost DC-DC converter in mobile applications: A comparison with a linear PID controller”. In: *2011 IEEE International Symposium of Circuits and Systems (ISCAS)*. 2011, pp. 1604–1607. DOI: 10.1109/ISCAS.2011.5937885.

[3] C. Albea, G. Garcia, and L. Zaccarian. “Hybrid dynamic modeling and control of switched affine systems: Application to DC-DC converters”. In: *2015 54th IEEE Conference on Decision and Control (CDC)*. 2015, pp. 2264–2269. DOI: 10.1109/CDC.2015.7402544.

[4] C. Albea Sanchez, O. Lopez Santos, D. A. Zambrano Prada, F. Gordillo, and G. Garcia. “On the Practical Stability of Hybrid Control Algorithm With Minimum Dwell Time for a DC–AC Converter”. In: *IEEE Transactions on Control Systems Technology* 27.6 (2019), pp. 2581–2588. DOI: 10.1109/TCST.2018.2870843.

[5] G. Beneux, P. Riedinger, J. Daafouz, and L. Grimaud. “Adaptive stabilization of switched affine systems with unknown equilibrium points: Application to power converters”. In: *Automatica* 99 (2019), pp. 82–91. DOI: 10.1016/j.automatica.2018.10.015.

[6] M. Benmiloud, A. Benalia, M. Djemai, and M. Defoort. “On the Local Stabilization of Hybrid Limit Cycles in Switched Affine Systems”. In: *IEEE Transactions on Automatic Control* 64.2 (2019), pp. 841–846. DOI: 10.1109/TAC.2018.2841806.

[7] Tongwen Chen and Bruce A. Francis. *Optimal Sampled-Data Control Systems*. 1st. Springer-Verlag London, 1995. DOI: 10.1007/978-1-4471-3037-6.

[8] D. Corona, J. Buisson, B. De Schutter, and A. Giua. “Stabilization of switched affine systems: An application to the buck-boost converter”. In: *2007 American Control Conference*. 2007, pp. 6037–6042. DOI: 10.1109/ACC.2007.4282539.

[9] G. S. Deaecto and J. C. Geromel. “Stability Analysis and Control Design of Discrete-Time Switched Affine Systems”. In: *IEEE Transactions on Automatic Control* 62.8 (2017), pp. 4058–4065. DOI: 10.1109/TAC.2016.2616722.

[10] G. S. Deaecto, J. C. Geromel, F. S. Garcia, and J. A. Pomilio. “Switched affine systems control design with application to DC-DC converters”. In: *IET Control Theory & Applications* 4.7 (2010), pp. 1201–1210. DOI: 10.1049/iet-cta.2009.0246.

[11] G. S. Deaecto, M. Souza, and J. C. Geromel. "Chattering free control of continuous-time switched linear systems". In: *IET Control Theory & Applications* 8.5 (2014), pp. 348–354. DOI: 10.1049/iet-cta.2013.0065.

[12] L. N. Egidio, H. R. Daiha, and G. S. Deaecto. "Global asymptotic stability of limit cycle and H2/H∞ performance of discrete-time switched affine systems". In: *Automatica* 116 (2020), p. 108927. DOI: 10.1016/j.automatica.2020.108927.

[13] L. N. Egidio, H. R. Daiha, G. S. Deaecto, and J. C. Geromel. "DC motor speed control via buck-boost converter through a state dependent limited frequency switching rule". In: *2017 IEEE 56th Annual Conference on Decision and Control (CDC).* 2017, pp. 2072–2077. DOI: 10.1109/CDC.2017.8263952.

[14] R. W. Erickson and D. Maksimović. *Fundamentals of Power Electronics.* 2nd. Springer US, 2001. DOI: 10.1007/b100747.

[15] F. S. Garcia, J. A. Pomilio, G. S. Deaecto, and J. C. Geromel. "Analysis and control of DC-DC converters based on Lyapunov Stability Theory". In: *2009 IEEE Energy Conversion Congress and Exposition.* 2009, pp. 2920–2927. DOI: 10.1109/ECCE.2009.5316085.

[16] M. Gildersleeve, H. P. Forghani-zadeh, and G. A. Rincon-Mora. "A comprehensive power analysis and a highly efficient, mode-hopping DC-DC converter". In: *Proceedings. IEEE Asia-Pacific Conference on ASIC,* 2002, pp. 153–156. DOI: 10.1109/APASIC.2002.1031555.

[17] Guisheng Zhai. "Quadratic stabilizability of discrete-time switched systems via state and output feedback". In: *Proceedings of the 40th IEEE Conference on Decision and Control (Cat. No.01CH37228).* Vol. 3. 2001, 2165–2166 vol.3. DOI: 10.1109/CDC.2001.980575.

[18] T. Hashemi, A. Farnam, R. M. Esfanjani, and H. M. Kojabadi. "A new approach to design switching strategy for the Buck converters". In: *4th Annual International Power Electronics, Drive Systems and Technologies Conference.* 2013, pp. 301–305. DOI: 10.1109/PEDSTC.2013.6506722.

[19] L. Hetel and E. Fridman. "Robust Sampled – Data Control of Switched Affine Systems". In: *IEEE Transactions on Automatic Control* 58.11 (2013), pp. 2922–2928. DOI: 10.1109/TAC.2013.2258786.

[20] W. Al-Hoor, J. A. Abu-Qahouq, L. Huang, and I. Batarseh. "Adaptive Variable Switching Frequency Digital Controller Algorithm to Optimize Efficiency". In: *2007 IEEE International Symposium on Circuits and Systems.* 2007, pp. 781–784. DOI: 10.1109/ISCAS.2007.378002.

[21] M. Z. Hossain, N. A. Rahim, and Jeyraj a/l Selvaraj. "Recent progress and development on power DC-DC converter topology, control, design and applications: A review". In: *Renewable and Sustainable Energy Reviews* 81 (2018), pp. 205–230. DOI: 10.1016/j.rser.2017.07.017.

[22] T. Konjedic, L. Korošec, M. Truntič, C. Restrepo, M. Rodič, and M. Milanovič. "DCM-Based Zero-Voltage Switching Control of a Bidirectional DC–DC Converter With Variable Switching Frequency". In: *IEEE Transactions on Power Electronics* 31.4 (2016), pp. 3273–3288. DOI: 10.1109/TPEL.2015.2449322.

[23] Liping Guo. "Implementation of digital PID controllers for DC-DC converters using digital signal processors". In: *2007 IEEE International Conference on Electro/Information Technology.* 2007, pp. 306–311. DOI: 10.1109/EIT.2007.4374445.

[24] Liping Guo, J. Y. Hung, and R. M. Nelms. "PID controller modifications to improve steady-state performance of digital controllers for buck and boost converters". In: *APEC. Seventeenth Annual IEEE Applied Power Electronics Conference and Exposition (Cat. No.02CH37335).* Vol. 1. 2002, pp. 381–388. DOI: 10.1109/APEC.2002.989274.

[25] L. Martínez-Salamero, G. García, M. Orellana, C. Lahore, and B. Estibals. "Start-Up Control and Voltage Regulation in a Boost Converter Under Sliding-Mode Operation". In: *IEEE Transactions on Industrial Electronics* 60.10 (2013), pp. 4637–4649. DOI: 10.1109/TIE.2012.2210375.

[26] C. A. Sanchez, G. Garcia, S. Hadjeras, W. P. M. H. Heemels, and L. Zaccarian. "Practical Stabilization of Switched Affine Systems With Dwell-Time Guarantees". In: *IEEE Transactions on Automatic Control* 64.11 (2019), pp. 4811–4817. DOI: 10.1109/TAC.2019.2907381.

[27] M. Serieye, C. Albea-Sanchez, A. Seuret, and M. Jungers. "Stabilization of switched affine systems via multiple shifted Lyapunov functions". In: *21st IFAC World Congress, IFAC 2020.* 2020.

[28] A. Sferlazza, C. Albea-Sanchez, L. Martínez-Salamero, G. García, and C. Alonso. "Min-Type Control Strategy of a DC–DC Synchronous Boost Converter". In: *IEEE Transactions on Industrial Electronics* 67.4 (2020), pp. 3167–3179. DOI: 10.1109/TIE.2019.2908597.

[29] T. Shi, Y. Guo, P. Song, and C. Xia. "A New Approach of Minimizing Commutation Torque Ripple for Brushless DC Motor Based on DC–DC Converter". In: *IEEE Transactions on Industrial Electronics* 57.10 (2010), pp. 3483–3490. DOI: 10.1109/TIE.2009.2038335.

[30] J. A. M. Silva, G. S. Deaecto, and T. A. S. Barros. "Analysis and Design Aspects of Min-Type Switching Control Strategies for Synchronous Buck-Boost Converter". In: *Journal of Emerging and Selected Topics in Power Electronics* (submitted).

[31] S. Tan, Y. M. Lai, and C. K. Tse. "General Design Issues of Sliding-Mode Controllers in DC–DC Converters". In: *IEEE Transactions on Industrial Electronics* 55.3 (2008), pp. 1160–1174. DOI: 10.1109/TIE.2007.909058.

[32] G. R. Walker and P. C. Sernia. "Cascaded DC-DC converter connection of photovoltaic modules". In: *IEEE Transactions on Power Electronics* 19.4 (2004), pp. 1130–1139. DOI: 10.1109/TPEL.2004.830090.

[33] F. Wu, X. Qu, C. Li, J. Lian, and L. Xu. "Multi-rate sampled-data control of switched affine systems". In: *IET Control Theory & Applications* 14.11 (2020), pp. 1524–1530. DOI: 10.1049/iet-cta.2019.0446.

[34] X. Yan, Z. Shu, S. M. Sharkh, Z. Wu, and M. Z. Q. Chen. "Sampled-data control with adjustable switching frequency for DC-DC converters". In: *IEEE Transactions on Industrial Electronics* 66.10 (2019), pp. 8060–8071. DOI: 10.1109/TIE.2018.2878116.